Adaptation of the CIMEL-318T to Shipborne Use: Three Years of Automated AERONET-Compatible Aerosol Measurements Onboard the Research Vessel Marion Dufresne

Benjamin Torres[1], Luc Blarel[1], Philippe Goloub[1], Gaël Dubois[1], Maria Fernanda Sanchez-Barrero[1], Ioana Elisabeta Popovici[1,2], Fabrice Maupin[2], Elena Lind[3], Alexander Smirnov[3,4], Ilya Slutsker[3,4], Julien Chimot[5], Ramiro González[6,7], Michaël Sicard[8,9], Jean Marc Metzger[10], and Pierre Tulet[11]

[1]Univ. Lille, CNRS, UMR 8518 - LOA - Laboratoire d'Optique Atmosphérique, F-59000 Lille, France.
[2]R&D Department, Cimel Electronique, 75011 Paris, France.
[3]NASA Goddard Space Flight Center (GSFC), Greenbelt, MD20771, USA.
[4]Science Systems and Applications, Inc. (SSAI), Lanham, MD20706, USA.
[5]EUMETSAT, 64295 Darmstadt, Germany.
[6]Group of Atmospheric Optics, University of Valladolid (GOA-UVa), 47011, Valladolid, Spain.
[7]Laboratory for Disruptive Interdisciplinary Science (LaDIS), Universidad de Valladolid, 47011 Valladolid, Spain.
[8]Laboratoire de l'Atmosphère et des Cyclones (LACy), UMR 8105 CNRS, Université de La Réunion, Météo-France, 97744, Saint-Denis de La Réunion, France.
[9]CommSensLab-UPC, Universitat Politècnica de Catalunya, Barcelona, 08034, Spain.
[10]OSU-R, CNRS/Université de La Réunion/Météo-France/IRD, UAR 3365, Saint-Denis, France.
[11]LAERO, UMR 5560 (CNRS, UT3, IRD), 31400, Toulouse, France.

Correspondence: Benjamin Torres (benjamin.torres@univ-lille.fr)

Abstract.

The Earth's oceans play a critical role in regulating the global climate and atmospheric processes, with marine aerosols significantly influencing weather patterns, air quality, and climate dynamics. Despite extensive land-based aerosol monitoring through networks like AERONET (AErosol RObotic NETwork), marine aerosol characterization remains a critical gap,

5　due in part to the logistical challenges of conducting measurements in remote oceanic environments. To address this, robust, automated, and precise monitoring systems adapted for research vessels are essential.

This study reports on the first three years (July 2021 to June 2024) of continuous aerosol optical depth (AOD) measurements collected aboard the Research Vessel Marion Dufresne using a ship-adapted CIMEL CE318-T automatic photometer in the frame of MAP-IO (Marion Dufresne Atmospheric Program - Indian Ocean) program. The dataset comprises over

10　25,000 quality-assured AOD measurements, primarily from the South-West Indian Ocean region, revealing mid-range AOD and Ångström exponent values consistent with previous studies. The reliability and precision of the system were validated through dual-instrument comparisons conducted during the Amaryllis-Amagas/Transama campaign, yielding strong correlations (R > 0.96 for different wavelengths) and low root-mean-squared errors (RMSE < 0.01), within the expected error margins for AERONET ground-based sites, and benefiting from the continue tracking system implemented for ship-adapted version.

15　Additionally, recurrent comparisons with the ground-based AERONET site at Saint-Denis (La Réunion) further confirm the

1

system's accuracy, presenting good correlations despite differences in altitude and the greater influence of local urban aerosols in Saint-Denis.

Retrievals from spectral AOD and sky radiance data collected over the Indian Ocean during a biomass burning event (October 2023) demonstrate the feasibility of deriving detailed aerosol properties, including size distribution and optical characteristics, from shipborne platforms adapted for marine conditions, following the protocols of the AERONET standard algorithm. Observed single scattering albedo (SSA) values, ranging from 0.88 to 0.95 with higher absorption at longer wavelengths, align with those recorded at the Saint-Denis site during the event and are consistent with expectations for a mixture of biomass burning (at the end of the dry season) and sea salt aerosols. These preliminary results underscore the potential of shipborne systems to provide comprehensive aerosol characterization in remote marine environments.

1 Introduction

Atmospheric aerosol optical studies, including radiative forcing analysis, aerosol-cloud interactions, remote sensing of the atmosphere, and global aerosol modeling, rely on precise information about AOD and aerosol absorption. Oceans, which cover approximately 70% of the Earth's surface, play a crucial role in the atmospheric system through sea-air interactions on both local and global scales. Specifically, oceans serve as a major source of sea spray aerosols and primary organic matter, such as chlorophyll-a (Gantt and Meskhidze, 2013). Sea spray aerosols, consisting of seawater droplets and dry sea salt particles (ionic species like sodium, potassium, etc.), are produced predominantly by bubble bursting from breaking waves (Blanchard and Woodcock, 1980). These particles range in size from 0.05 μm to 1 mm (Hoppel et al., 1990; O'Dowd et al., 1997; Porter and Clarke, 1997). The production of sea spray is influenced by factors such as wind speed, sea state, atmospheric stability, and seawater composition (O'Dowd and Smith, 1993; de Leeuw et al., 2011). Globally, sea spray aerosols are the dominant contributors to columnar AOD over oceans (Mahowald et al., 2006), and are the most widely dispersed natural aerosols with an estimated total flux of 4100 Tg yr^{-1} according to the IPCC-2013 (Stocker et al., 2013). The contained primary marine organic matter is normally found in smaller particles under 200 nm (Leck and Bigg, 2008; Russell et al., 2010), with emission rates dependent on biological activity in ocean waters, estimated between 2 and 20 Tg yr^{-1} (Facchini et al., 2008; Gantt et al., 2011). From a climatic perspective, the main interest in sea spray aerosols lies in their direct influence on the radiation budget due to their predominantly scattering nature (Gordon and Clark, 1981; Gathman, 1983; Haywood et al., 1999; Satheesh and Krishna Moorthy, 2005), as well as their indirect impact on cloud formation, dynamics, and life cycle, driven by their hygroscopic properties (e.g., Gunn and Phillips, 1957; Albrecht, 1989; O'Dowd et al., 1999; Van den Heever et al., 2006; Sandu et al., 2008).

Characterizing marine environments is particularly challenging due to the complexity of aerosol production and the variety of sources involved (Lewis and Schwartz, 2004). Marine atmospheric aerosols encompass both the natural components mentioned above emitted by the sea and aerosols transported from terrestrial sources, whether natural (e.g., desert dust) or anthropogenic (e.g., sulfates, nitrates, or biomass burning aerosols, see Prospero et al., 2002; O'Dowd and de Leeuw, 2007; O'Dowd et al., 2007). These aerosols contribute to the complex and dynamic nature of marine environments. For example, long-range transport

of continental aerosols modifies the aerosol composition over the ocean, blending natural sea salt with desert dust or industrial

50 emissions (Fitzgerald, 1991; O'Dowd et al., 2007). The generally low concentrations of marine aerosols make their climatic effects highly sensitive to small changes. As Koren et al. (2014) suggested, even minor variations can significantly influence cloud formation and radiative forcing, often resulting in negative forcing (cooling) by promoting convective cloud development.

Pristine marine regions, such as the Southern Indian Ocean and the South Pacific, are particularly valuable for understanding these processes because there is minimal human influence on them (Hamilton et al., 2014). Studying aerosols in these regions

55 also provides information on preindustrial meteorological conditions, which serve as a baseline to evaluate the contribution of natural emissions to climate change. Furthermore, recent findings highlight the role of marine aerosols in climate feedback mechanisms, with processes such as marine cloud brightening (Alterskjær and Kristjánsson, 2013), illustrating the sensitivity of radiative forcing to aerosol-cloud interactions (Twomey, 1977). However, the efficacy of such processes is influenced by meteorological conditions, background aerosol levels, and particle properties, resulting in a wide range of potential impacts

60 on radiative forcing, estimated between -5.4 and -0.8 W m^{-2} (Intergovernmental Panel on Climate Change (IPCC), 2021, mostly based on the analysis by Pringle et al., 2012).

Despite advances in understanding marine aerosols, substantial uncertainties continue to exist due to their strong dependence on sources, emissions, and interactions with clouds. Variability in sea spray concentrations, driven by changes in wind speed, sea state, and sea ice cover, adds further complexity (Struthers et al., 2011). Climate projections suggest that these emissions

65 could increase or decrease under changing conditions, with potential implications for aerosol-cloud-climate feedbacks (Jones et al., 2007). Addressing these uncertainties requires comprehensive observational datasets to refine models, improve estimates of aerosol sources, and better quantify their climatic impacts. Systematic measurements of aerosol optical properties in maritime environments, coupled with robust statistical analysis, are therefore essential to advance our understanding of regional marine aerosol climatologies, their trends, and their global effects.

70 Marine aerosol optical properties can be measured using passive remote sensing instruments from spaceborne, airborne, or shipborne platforms. Spaceborne observations offer a global, long-term perspective on marine aerosol conditions, with aerosol properties retrieved by analyzing spectral radiances collected by their sensors from solar reflection off the Earth's surface and transmission through the atmosphere. In this context, satellite data retrievals either rely on assumptions about surface reflectance or employ a combined retrieval of aerosol and surface properties (Dubovik et al., 2011; Sayer et al., 2018), both

75 of which introduce non-negligible errors. The accuracy and level of detail of aerosol products derived from satellite data vary depending on sensor performance and capabilities (e.g., multi-wavelength, multi-angular, and polarization measurements). For the most advanced sensors, AOD uncertainties at 550 nm typically start at 0.04–0.05 over oceans and around 0.1 over land (see, for example, validation studies in Gupta et al., 2018; Dubovik et al., 2019; Chen et al., 2020).

In contrast, AOD from Earth-based measurements is obtained through direct irradiance measurements of the Sun (or Moon)

80 using precise photometers and applying the well-known Beer–Bouguer–Lambert law (Shaw, 1983), which describes the attenuation of solar or lunar light as it passes through the atmosphere. The associated uncertainty is around 0.01 to 0.02 and is mainly due to errors in the calibration coefficient in the different channels (Eck et al., 1999; Holben et al., 2006; Giles et al., 2019), a level significantly lower than that of satellite-derived AOD products. The high precision of Earth-based measure-

ments is particularly valuable for improving our understanding of regional marine aerosol properties and their climatologies, while also refining uncertainty estimates for satellite aerosol products over oceans. These satellite products are rarely validated with Earth-based data due to a critical lack of ground observations in oceanic regions. In most validation studies, available data usually come from island stations or coastal sites, rather than from pure open-ocean environments. Additionally, this lack of Earth-based data in oceanic areas also complicates the validation of aerosol transport models, which typically rely on ground-based data to extend coverage of detailed aerosol properties beyond fixed ground-based sites. This gap in validated marine aerosol data hinders a comprehensive understanding of general aerosol dynamics and impedes accurate global climate predictions.

One reason for the lack of data over oceans is that most aerosol ground-based networks have historically concentrated on studying aerosol properties over land. For example, the well-known AERONET network (Holben et al., 1998, 2001) comprises more than six hundred land-based sites, with limited information over the oceans, primarily covering islands. However, not all areas of the World Ocean can be studied from islands; aside from space and airborne sensors, ships are the only platforms where measurements can be obtained. Consequently, despite challenges such as platform mobility and the harsh marine environment, including exposure to salt and high humidity, shipborne sun photometer observations have advanced significantly over the past 20 years (see for example developments for Prede POM instruments at Kobayashi and Shiobara, 2015). The largest long-term aerosol observation network in the ocean is the Maritime Aerosol Network (MAN) (Smirnov et al., 2009), a component of AERONET. MAN inherits its legacy from the NASA SIMBIOS (Sensor Intercalibration and Merger for Biological and Interdisciplinary Oceanic Studies) program (Fargion et al., 2000, 2003; Knobelspiesse et al., 2004). MAN provides a unique data set of AOD, the Ångström exponent (as defined by Ångström (1929) and calculated within using a least-squares linear regression in log–log space over the 440–870 nm wavelength range), and precipitable water vapor (PWV) in the ocean, spanning from the Arctic to Antarctica.

MAN exploits the advanced AERONET calibration facilities and processing schemes and relies on many logistical and scientific developments from the AERONET Project. The MAN web-based public data archive is available from the AERONET website. MAN represents an important strategic sampling initiative, and ship-borne data acquisition complements island-based AERONET measurements. MAN started collecting data over the oceans in November 2006 and has since made significant progress in data collection and archival. With more than 750 cruises completed and ongoing (and many more planned), the MAN database continues to grow, enhancing our knowledge of spectral AOD variation over the oceans. The ultimate objective is to advance the fundamental scientific understanding of aerosol optical properties globally through highly accurate and standardized measurements, providing a basis for evaluation and inter-comparison of AOD retrievals from various spaceborne sensors and outputs of the global aerosol transport models. However, unlike AERONET ground-based standard instruments, the standard device of MAN is the hand-held Microtops II Sun photometer, which requires manual operation, making it less suitable for continuous and unattended measurements. Furthermore, it cannot provide aerosol optical and microphysical properties obtained through the AERONET aerosol retrieval algorithm (Dubovik and King, 2000; Dubovik et al., 2000, 2002b, 2006; Sinyuk et al., 2020) due to the lack of sky radiance measurements (Smirnov et al., 2009).

For these reasons, the development of a ship-adapted version of the automated standard instrument used at AERONET ground-based sites, the CIMEL CE318-T Sun/Moon photometer (from now referred only as CE318-T), has been a primary objective in recent years within the Agora Lab framework (CIMEL Electronique and Université de Lille, https://www.agora-lab.fr, last access: 31 May 2025). The aim is to acquire aerosol properties from moving platforms using the same protocols and standards as those applied at AERONET ground sites. This strategy ensures consistency across the network and enables the retrieval of high-quality shipborne data.

This paper presents the technical development of the fully autonomous, AERONET-compatible version of the CE318-T Sun photometer for deployment on oceanographic research vessels. Section 2 details the evolution and final architecture of the system, while Section 3 reports on three years of continuous AOD measurements from the Research Vessel (R.V.) Marion Dufresne, the first ship to host such a system. Section 4 introduces the first shipborne AERONET retrievals of aerosol microphysical and optical properties. Throughout the paper, data validation and performance analysis are conducted with the objective of demonstrating that shipborne measurements can achieve the same level of quality and standardization as those from land-based AERONET sites. This opens the possibility of integrating shipborne data into global aerosol networks, thereby extending coverage to remote oceanic regions and supporting satellite validation and climate modeling efforts.

2 Instrument, site and data treatment

2.1 Sea-deployed CE318-T photometer

2.1.1 System adaptation and historical development

Adapting the CE318-T for shipborne use required two key modifications, both identified during the early stages of development. The first was the integration of real-time attitude information (specifically, GPS position, heading, pitch, and roll) to allow the instrument to continuously compute the Sun or Moon position relative to the moving platform. This capability became feasible with the modernization introduced in the CE318-T version (Barreto et al., 2016), which includes an internal GPS receiver capable of automatically determining geographic coordinates (an improvement over previous models that required manual entry). In the shipborne configuration, GPS updates are acquired every five minutes, compared to once daily in standard ground-based operation. While the internal GPS provides accurate location data, additional attitude parameters (heading, pitch, and roll) are supplied by an external system. In the last version of CE318-T, control electronics and software can be updated accordingly to allow integration of this external attitude information, enabling real-time compensation for platform motion.

The second essential modification was the implementation of continuous Sun (or Moon) tracking during direct irradiance measurements. In ground-based sites, the instrument tracks the Sun (or Moon) only once prior to each triplet measurement sequence (comprising three repetitions over nine spectral channels, as detailed in subsection 2.2). On a moving platform, however, continuous tracking is necessary to maintain alignment throughout the acquisition period and to ensure accurate AOD measurements despite vessel movement.

These core modifications enabled the first successful experiments with shipborne CE318-T operation during the AQABA campaign in 2017, onboard the R.V. Kommandor-Iona (Eger et al., 2019; Kaskaoutis et al., 2023; Pfannerstill et al., 2019), around the Arabian Peninsula. To obtain the vessel's attitude information, previous experience from developing photometry on moving platforms was leveraged. Specifically, the magnetic compass developed for the PLASMA airborne photometer (Karol et al., 2013) was used in this first implementation to compute the magnetic declination. The system operated successfully and produced the first automatic AOD measurements with CE318-T on a ship, during the transit from southern France to Kuwait (Unga et al., 2019). However, several operational limitations were soon identified. First, the magnetic compass required frequent recalibration to account for the magnetic environment of the ship. This procedure is feasible for short airborne deployments (as it is routinely performed before each PLASMA flight), but is impractical for long-term autonomous shipboard operations. In addition, the software did not include magnetic declination information, which is essential for the proper functioning of the heading calculation. Second, sea spray caused water ingress and salt deposition on the optics, revealing the need for a protective system to shield the collimator. Third, the CE318-T standard resistive rain sensor was found to be unsuitable for marine conditions, as it oxidized. Finally, strong winds and high waves not only increased instrument motion but also created risks of water ingress into the sensors, underscoring the need for a wind monitoring system capable of disabling measurements under harsh conditions.

These challenges informed a series of improvements implemented during subsequent deployments in the OCEANET transatlantic campaigns (PS113, PS116, and MOSAIC/Arctic) aboard the R.V. Polarstern (Yin et al., 2019). A protective system known as the "airshield" (a general term for the anti–sea spray setup using continuous air injection) was introduced. In this first implementation, dry air was channeled from inside the vessel to the base of the CE318-T collimator in order to prevent sea spray contamination. While this solution effectively shielded the optics from marine aerosols and salt deposition, condensation issues occasionally occurred due to differences in temperature and humidity between the interior of the vessel and the external environment. To enhance durability in marine conditions, the original resistive rain sensor was replaced with a corrosion-resistant optical sensor. An anemometer was also added to monitor wind speed and automatically disable measurements during strong winds. Furthermore, the basic electronic card-based attitude measurement system (magnetic declination calculator) was replaced by a SIMRAD-H60 commercial navigation compass, which includes a dual GPS antenna and a declination-corrected magnetic compass. These combined enhancements significantly improved the quality and quantity of retrieved AOD products. Yin et al. (2019) reported strong agreement between the CE318-T and the handheld MAN Microtops-II instrument, with RMSE of 0.015, 0.013, 0.010, and 0.009 at 380, 440, 500, and 870 nm, respectively, and correlation coefficients (R) of 0.99 at all wavelengths.

However, despite testing two versions of the SIMRAD-H60 system during the campaigns on the R.V. Polarstern (MOSAIC/Arctic campaign), attitude errors ranging between 2–$5°$ occasionally complicated the Sun acquisition, as the field of view of the CE318-T tracking system is approximately $3°$. This solution proved insufficient for the intended fully autonomous system, where the instrument can be deployed for several months at sea without continuous supervision.

The final improvements leading to the current version were implemented in 2020 (note that all technical components of the present system are described in detail in subsection 2.1.2). During the Sea2Cloud campaign aboard the R.V. Tangaroa, the

SIMRAD-H60 system was replaced with the ABX-Two inertial GPS unit, ensuring a RMSE of 0.07–0.1° for heading and 0.13–0.2° for pitch and roll[1]. The system functioned correctly after some initial adjustments to the position of the antennas. Unfortunately, only a few AOD measurements were obtained since the campaign started on March 1, 2020, and was canceled by the end of the month due to the COVID-19 pandemic. In late 2020, additional tests were conducted on fishing boats (small vessels of around 20 meters in length) off the coast of northern France. The fishing boats conducted daily round trips, allowing for numerous tests and on-site modifications. During these tests, the final airshield system was installed outside, effectively preventing condensation issues. Additionally, the CE318-T firmware was adapted to enable automatic radiance (Almucantar) measurements for the ship-version.

By early 2021, the goal was to install a fully AERONET-compatible photometer on the R.V. Marion Dufresne (a vessel of the French oceanographic fleet), as part of the MAP-IO program (Tulet et al., 2024). More details about the vessel and the MAP-IO project are provided in subsection2.3. The instrument included all necessary adaptations for marine operations, along with the final software version capable of performing both direct and radiance measurements. However, a calibration issue was identified during installation. As a result, a different photometer, running an earlier software version, was installed and provided the first measurements onboard the R.V. Marion Dufresne. This instrument, operational from January to March 2021, routinely performed automatic AOD measurements, while radiance measurements were taken manually, as it lacked the updated system for automatic sky radiance acquisition. The initially planned instrument was subsequently recalibrated and, on 1 July 2021, the first fully AERONET-compatible photometer deployed at sea was successfully installed onboard the R.V. Marion Dufresne, marking a significant milestone. This deployment serves as the reference point for the data analyzed in this study, collected using the fully operational and network-compliant shipborne system.

2.1.2 Current version and implementation

With all the aforementioned developments, the current system has evolved into a robust, modular configuration incorporating the necessary adaptations for long-term autonomous operation aboard research vessels. The present version combines the CE318-T photometer with an inertial GPS unit, a protective airshield, and a weather control system to ensure continuous, reliable measurements at sea. A schematic overview of this final modular configuration is provided in Figure 1, and its components are described in detail below.

The core of the system is the CE318-T Sun photometer (center of Figure 1), the latest standard instrument in the AERONET network. It performs automated measurements of spectral AOD (340 to 1640 nm), downward sky radiances (380 to 1640 nm), and column-integrated water vapor content, following the same protocols as AERONET ground-based sites. The second key component is the Trimble ABX-Two inertial GPS unit (shown on the right side of Figure 1), which provides real-time attitude

---

[1] The specifications of the ABX-Two inertial GPS unit indicate an RMSE of 0.1° per meter of baseline (distance between the antennas) for heading and 0.2° for pitch and roll. Given that the final antenna separation aboard the R.V. Marion Dufresne ranged from 1.5 to 2 meters, the associated errors fall within these stated values. Internal tests conducted on fixed platforms confirm these specifications. In contrast, the specifications for the SIMRAD-H60 system indicate a RMSE of 2° (with 68% of values below this threshold); however, similar internal tests have revealed larger errors in practice, reaching up to 5° as stated in the text.
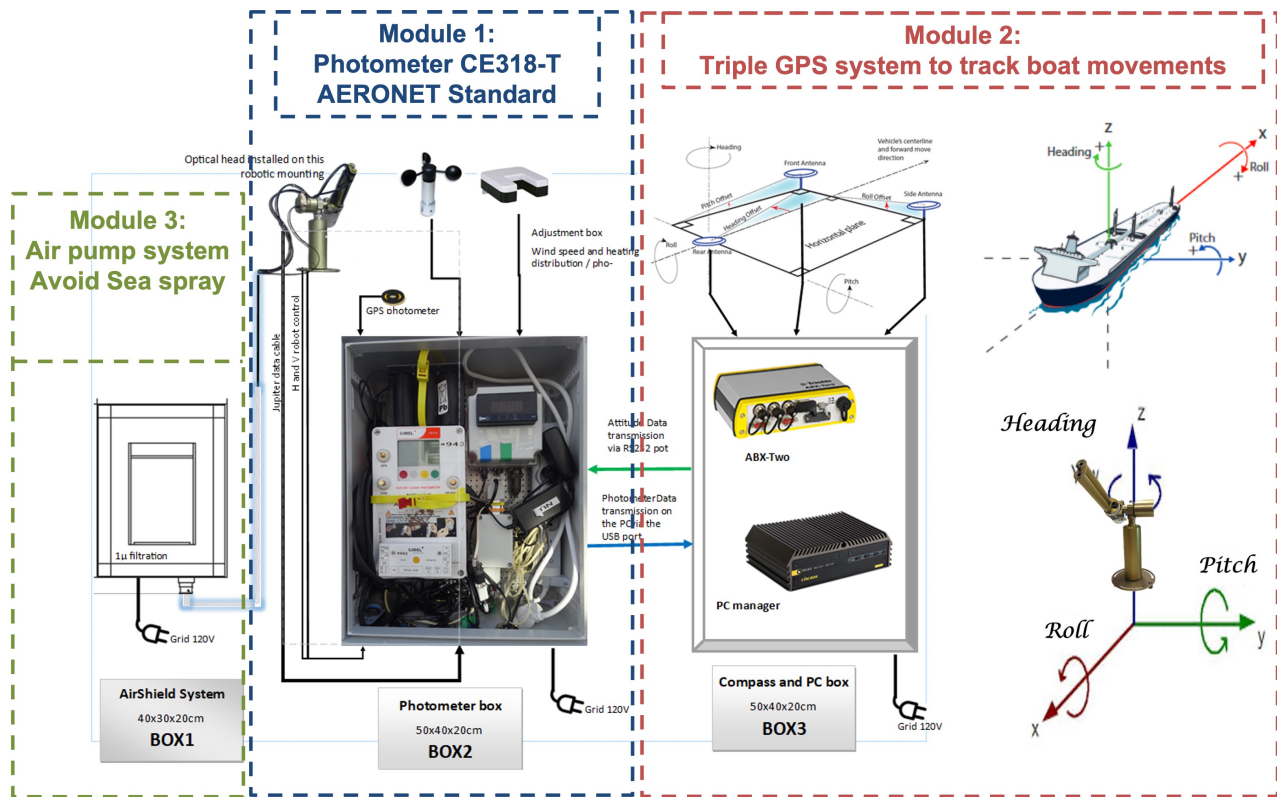
Figure 1. Scheme of the photometer adapted for boat conditions. The central part of the figure shows the CE318-T photometer, the latest standard instrument in the AERONET network, originally designed for ground-based installations. The right side displays the Trimble ABX-Two inertial GPS unit, which provides attitude data (heading, roll, pitch) and continuously transmits this information to the photometer's communication ports. The left side of the figure illustrates the airshield, which supplies clean, compressed air to the base of the collimator, preventing sea spray deposition. A weather system, including a non-corrosive optical rain sensor and an anemometer, is also integrated to halt operation during rain or high winds. Source: Pictures of Module 3 taken from the User Guide of the Trimble ABX-Two.

information with an estimated uncertainty below $0.2°$. This data is continuously transmitted to the photometer and, together with its internal GPS position, allows the system to compute the Sun and Moon positions relative to the moving platform with high precision. Once the Sun or Moon enters the field of view of the tracking system, the photometer engages the adapted continuous tracking mode for shipborne operation, ensuring stable alignment throughout acquisition despite vessel motion. In addition, the ABX-Two generates continuous positioning data, which, together with attitude information, are recorded every second on a dedicated PC. This PC also collects data from the photometer and manages connectivity with the ship's communication system (Wi-Fi/cable),facilitating remote access and monitoring.

To prevent sea spray contamination, an airshield (located on the left side of Figure 1) supplies clean, dry air to the base of the photometer's collimator. This airflow creates a protective overpressure that prevents both sea spray deposition and particle

intrusion. A flexible, butyl-lined hose connects the pump to the photometer, minimizing pressure loss while allowing free movement of the tracking head. A filter installed at the air intake (Box1) ensures that only clean air flows through the system. The pump operates continuously to protect the optics, even when measurements are paused, although it can be manually stopped when the head is removed.

The system also includes a weather unit with a corrosion-resistant optical rain sensor and an anemometer to monitor wind speed. Measurements are automatically halted during precipitation or high winds, protecting the instrument from sea spray (due to wave splash) and excessive motion. The unit is connected through the standard humidity sensor port and follows an enhanced safety protocol compared to land-based systems, which only pause measurements during rain.

Although a formal cost-benefit analysis is beyond the scope of this study, the operational feasibility of the system has been demonstrated through multi-year deployments with only minor repairs. The shipborne CE318-T system operates autonomously, occupies minimal deck space, and requires a standard 220V power supply, with a maximum consumption below 100 W. All components (photometer, airshield, control units, and inertial GPS units) are compact and lightweight, with installation requiring about one full day by two trained personnel. The system can be affixed to standard ship railings using stainless steel clamps with rubber padding, ensuring stability under marine conditions. Maintenance is minimal—mostly limited to occasional filter cleaning and visual inspections— while continuous data transmission (maximum 5 kilobytes per hour for near-real-time data processing) and remote diagnostics (e.g., via TeamViewer) enable reliable, unattended operation for several months at sea. These characteristics make the current system design scalable and well suited for broader deployment aboard other research vessels, particularly within global ocean monitoring frameworks. Finally, it is important to note that the Trimble ABX-Two system is currently facing supply constraints. Finally, it is important to note that the Trimble ABX-Two system is currently facing supply constraints. Although it remains a key component of the architecture shown in Figure 1, alternative commercial solutions are being evaluated to ensure comparable attitude precision and performance, with minimal impact on cost and overall system design.

The installation position aboard the vessel is selected in coordination with the crew to ensure optimal sky visibility (i.e., minimal obstruction from ship structures), while also considering other aspects such as ease of access, avoiding proximity to exhausts or contamination sources, mounting the system at a sufficient height to reduce exposure to waves, and avoiding electromagnetic interference from large antennas, which may affect the Trimble ABX-Two. In particular, the position on the R.V. Marion Dufresne, shown in Figure 1 of Tulet et al. (2024), has proven effective in maintaining consistent solar acquisition while protecting the instrument from spray and mechanical interference.

2.2 Data Processing and Availability

2.2.1 Acquisition, calibration and treatment

The use of the standard CE318-T photometer in the shipborne system offers a major advantage: its full compatibility with AERONET calibration and processing protocols. This compatibility ensures that the same quality control and quality assurance (QC/QA) procedures can be applied to all measurements, significantly simplifying the data treatment workflow. The term

"AERONET-compatible" implies that the shipborne photometers follow the same measurement protocols and schedules as ground-based instruments, use identical optical filters, and undergo the same calibration and data processing. In particular, the calibration of both irradiance (Sun and Moon direct measurements) and sky radiance is performed using the same methods as for terrestrial photometers, ensuring consistency and comparability across the network.

Solar irradiance calibration is conducted through intercomparisons with reference "master" photometers at dedicated calibration facilities operated by NASA Goddard (USA), the University of Lille (France), the University of Valladolid (Spain), and the Asia Pacific AERONET Calibration and Training Center (APAC, Taiwan). These master instruments are themselves calibrated using the Langley plot method at high-altitude sites such as Mauna Loa and Izaña, where atmospheric conditions are stable and aerosol loads are minimal (see Toledano et al., 2018). The resulting calibration coefficient, commonly referred to as the "extraterrestrial constant," corresponds to the digital number (DN) that the instrument would produce under extraterrestrial irradiance, that is, the expected output signal from the photodetector if the measurement were taken at the top of the atmosphere, with no atmospheric attenuation. This coefficient is then used to derive AOD through the Beer–Bouguer–Lambert law (Shaw, 1983; Holben et al., 1998) and the direct Sun/Moon measurements. In contrast, sky radiance calibration is carried out in controlled laboratory conditions using an integrating sphere. Regular recalibration (typically every 12 to 18 months) is required to compensate for instrument aging, particularly filter degradation, and to ensure long-term consistency.

Once the raw data are collected aboard the R.V. Marion Dufresne, they are transmitted via satellite to the PHOTONS CNRS National Observation Service (University of Lille), and subsequently forwarded to the NASA AERONET server. There, the data are processed using the AERONET Version 3 system, identical to that applied at ground-based sites. This includes rigorous quality-control protocols for assigning data to different quality levels (Level 1.0 and Level 1.5), as detailed in Giles et al. (2019). The most relevant steps and concepts for this analysis are briefly revisited and contextualized in the following subsections.

Unlike ground-based photometers, not all raw data from the shipborne instrument are automatically processed. Following an approach similar to that of the MAN program, only direct Sun or Moon measurements (used to derive spectral AOD, water vapor content, and the Ångström Exponent) are processed when the vessel is officially on mission. This avoids unnecessary processing during extended docked periods. However, some data collected while the ship is at port are still processed, particularly during declared testing missions involving daily departures and returns. Additionally, on certain days within declared testing periods, the vessel may remain at the dock while data continue to be processed. In the three-year dataset analyzed in this study, approximately 20% of the processed data correspond to periods when the vessel was within the port area[2]. These data, which include both daytime and nighttime measurements, are included in the analysis presented in subsection 3.1.

As part of the standard AERONET processing, Ångström Exponent (α) values are derived from the spectral dependence of AOD using the Ångström law (Ångström, 1929). Several α values are computed over different spectral intervals. In this study, we use the α calculated over the 440–870nm range, as it is the most commonly adopted in the literature and in AERONET-related studies. This value is obtained via log–log linear regression of all available AODs within this range (typically includes AOD at 440, 500, 675, and 870 nm) against wavelength.

---

[2]The ship does not always remain stationary while at port; the port area is considered to span approximately one square km.

2.2.2 Correct functioning and Level 1.0 assignment

Level 1.0 assignment is primarily based on the analysis of the instrument's electronic signal. Anomalies in system electronics (such as extreme battery voltages, amplifier malfunctions, or very low signal levels) can prevent measurements from reaching Level 1.0 (Giles et al., 2019). However, the most relevant criterion in this study is the verification of correct Sun (or Moon) pointing, which may be compromised by cloud obstruction or tracking system errors. This verification is based on the fact that AOD is derived using the Beer–Bouguer–Lambert law from a triplet of direct irradiance measurements. To ensure the reliability of these measurements, the relative RMSE of the DN triplet must remain below 16%; otherwise, the entire observation is discarded (see section 3.1.3 in Giles et al., 2019). In the case of the shipborne photometer, tracking errors, often associated vessel motion and vibrations, can lead to inconsistencies within the triplet, preventing the data from passing this 16% threshold.

Approximately 30% of the total Sun/Moon triplets from the shipborne photometer aboard the R.V. Marion Dufresne achieved Level 1.0 during the analyzed period (July 1, 2021 – June 30, 2024). Since the R.V. Marion Dufresne regularly operates near La Réunion, the AERONET site "REUNION_ST_DENIS" (hereafter Saint-Denis), located on the roof of the University of La Réunion at 93 meters above sea level, provides a relevant ground-based reference. For the same period, approximately 47% of the measurements at Saint-Denis reached Level 1.0. Given that Level 1.0 assignment is strongly influenced by instrument location and local climate conditions (e.g., obstruction by thick clouds), this comparison offers valuable context. Still, this difference is reasonable considering the additional challenges faced by shipborne measurements, particularly due to the vessel's motion and rotational movements. Moreover, part of the data loss can be attributed to installation-specific constraints. Unlike AERONET ground-based stations, which are typically located at sites with an unobstructed 360-degree horizon, shipborne platforms are subject to obstructions from onboard structures, masts, and other equipment intrinsic to the vessels. As mentioned earlier, the photometer position aboard the R.V. Marion Dufresne (see Figure 1 of Tulet et al. (2024)) was carefully chosen in coordination with the crew as the most suitable location for this vessel, though it places the instrument near a platform structure, further reducing the fraction of successful Level 1.0 measurements. Taking these constraints into account, the 30% success rate compared to 47% at Saint-Denis highlights the robustness of the shipborne system and its capability to maintain tracking in a high percentage of cases, even under challenging conditions.

2.2.3 Cloud screening and Level 1.5 assignment

While the 16% DN triplet variance test used for Level 1.0 assignment effectively filters out thick clouds and outliers, it is insufficient for detecting thin or homogeneous cloud layers such as cirrus. Achieving Level 1.5 (cloud-screened AOD data) therefore requires additional screening procedures. In AERONET Version 2, the main method was the AOD triplet variability test, which assessed fluctuations within each AOD triplet. A triplet was accepted if the difference between maximum and minimum AOD remained below 0.02 across all wavelengths. In cases of high aerosol loading (such as biomass burning or extreme haze events), a more flexible threshold was applied, allowing a maximum variability of $0.03 \cdot$ AOD, with the less restrictive criterion taking precedence when necessary.

320   AERONET Version 3 (Giles et al., 2019) introduced key refinements. First, the test was limited to three wavelengths (675, 870, and 1020 nm), avoiding unnecessary exclusions at shorter wavelengths where fine-mode aerosol can exhibit greater natural variability (Eck et al., 2018). At the same time, the threshold was made stricter: the AOD variability must remain below the greater of 0.01 or $0.015 \cdot$ AOD across all three wavelengths. Additional criteria were introduced, including refined temporal variation thresholds (see Table 2 in Giles et al., 2019), along with others highlighted by Giles et al. (2019). These

325   advancements further refine the cloud screening process in Version 3, enabling a more effective removal of cloud-contaminated data and enhancing the quality of Level 1.5 AOD measurements. Consequently, the Level 1.5 AOD data collected aboard the R.V. Marion Dufresne and presented here have undergone rigorous cloud screening, ensuring that the retained Sun and Moon measurements comply with AERONET's quality standards. Approximately 70% of the Level 1.0 data advance to Level 1.5, while this percentage is slightly higher at the Saint-Denis site reaching nearly 80%. The 10% difference is likely due to

330   occasional small tracking instabilities at sea, which may cause triplets to pass the 16% DN test but fail the more stringent 2% AOD triplet variability threshold.

While Level 2 quality-assured AOD data are routinely performed and available for AERONET ground-based instruments, shipborne data are currently limited to Level 1.5 due to the added complexity of operating on a moving platform. Further validations, such as that presented here and by Yin et al. (2019), remain essential for establishing the reliability of CE318-T

335   shipborne data within the AERONET network.

2.2.4 Sky radiances and inversion

The determination of calibrated downward atmospheric radiances from sky measurements acquired in almucantar geometry is processed during declared mission periods. Although the T-Model version of the CIMEL photometer is capable of performing hybrid sky scans —combining simultaneous azimuthal and zenith angle movements to provide intermediate data between

340   almucantar and principal plane geometries (Sinyuk et al., 2020)— the photometer installed aboard the R.V. Marion Dufresne is currently limited to almucantar scans due to its specific software configuration. This limitation, while restricting hybrid scan capabilities, remains fully AERONET-compatible and capable of producing high-quality sky radiance measurements. As with other regular AERONET instruments in the network, almucantar scans consist of azimuthal sweeps from $-180°$ to $+180°$, performed sequentially at four wavelengths (440, 675, 870, and 1020 nm). These scans are typically carried out in the morning

345   and afternoon at specific optical air masses of 3.8, 2.9, 2.0, 1.7, and 1.4, which correspond to solar zenith angles (θ_S) of 75°, 70°, 60°, 54°, and 45°, respectively.

Almucantar sky radiance data, combined with spectral AOD measurements at identical wavelengths, serve as input to the AERONET inversion algorithm developed by Dubovik and King (2000) and later expanded by Dubovik et al. (2006). This algorithm retrieves column-integrated, optically equivalent volume size distributions and aerosol refractive indices, which are

350   further utilized to derive secondary aerosol properties such as SSA, the asymmetry parameter, and phase functions. For the first time, this methodology has been applied to perform such retrievals from a shipborne platform within the AERONET network. However, retrievals from shipborne platforms are not yet automated. Processing has been done for selected periods of interest, and the first results are discussed in this study (section 4). Although all ground-based quality control criteria, including the
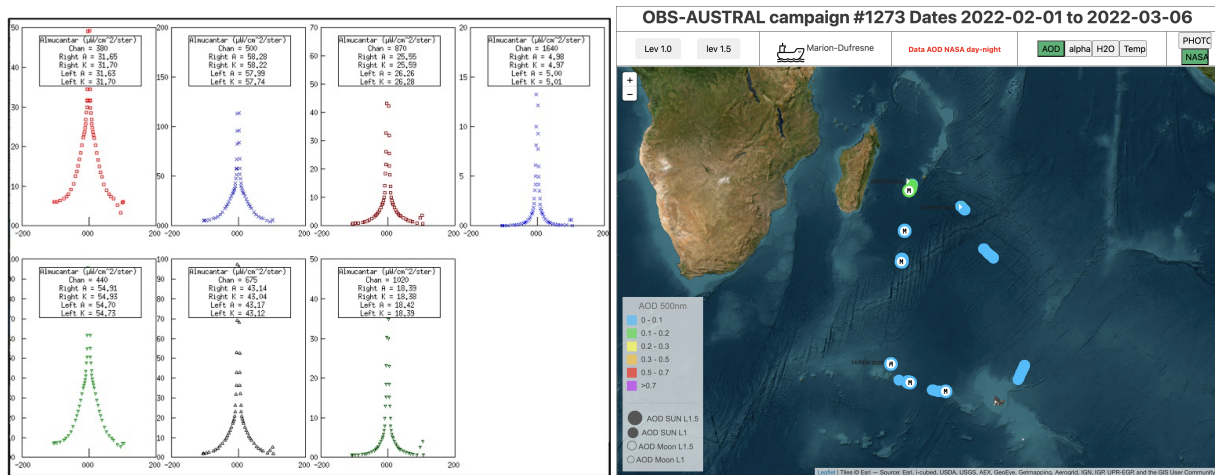
Figure 2. Left: Example of calibrated radiance measurements following an almucantar scenario on October 17, 2023, onboard the R.V. Marion Dufresne from Demonstrat (AERONET internal system). Right: Visualization of AOD_{440} during the OBS-AUSTRAL campaign from January to March 2022, as displayed on the PHOTONS system platform (https://mobile.photons.univ-lille.fr/, last access: 31 May 2025).

symmetry of almucantar scans, are considered in these initial inversions, additional quality criteria for shipborne retrievals are being analyzed. This includes setting extra thresholds related to ship motion during sky radiance acquisitions (or accounting for their effects), improving the model of sea water reflectances, and other factors.

2.2.5 Availability

AOD, water vapor, calibrated radiance, and preliminary aerosol microphysical and optical properties of the first AERONET retrievals are currently accessible internally through Demonstrat, an internal AERONET software used to aid calibration, technical control of equipment, and data review. Figure 2 (left) shows an example of calibrated radiance measurements from an almucantar scan performed on October 17, 2023, onboard the R.V. Marion Dufresne. These data will soon be accessible on the general AERONET website (https://aeronet.gsfc.nasa.gov, last access: 31 May 2025). This delay is due to the technical modifications required for the visualization software to handle data from moving platforms, as opposed to ground-based sites. In addition to AERONET processing and archiving, a near-real-time visualization system has been developed within the PHOTONS system (https://mobile.photons.univ-lille.fr/, last access: 31 May 2025). By selecting the mission and the boat, it is possible to visualize and download the corresponding AOD data (see the right panel of Figure 2, showing the AOD at 440 nm (AOD_{440}) during the OBS-AUSTRAL campaign from January to March 2022 as visualized through the PHOTONS system.).

2.3 R.V. Marion Dufresne and MAP-IO program

The R.V. Marion Dufresne is a state-of-the-art oceanographic research vessel operated by the French Research Institute for Exploitation of the Sea (Ifremer) for approximately 220 days per year, and by Terres Australes et Antarctiques Françaises

(TAAF) for around 120 days. The remaining time, typically about 25 days per year, the vessel remains at port for freight operations and routine maintenance activities such as mechanical repairs and technical upgrades. This period is also used for the maintenance and recalibration of scientific instruments installed on board. Designed for long-range, multidisciplinary scientific campaigns, the vessel is equipped with advanced laboratories and cutting-edge technologies, making it an ideal platform for atmospheric aerosol studies in marine regions.

The MAP-IO program, launched in early 2021, aims to address the critical lack of atmospheric and oceanographic observations in the Southern Indian and Southern Oceans—key regions in global climate regulation that remain among the least studied. By the end of 2024, after approximately 1100 days at sea, MAP-IO will have deployed 17 scientific instruments aboard the R.V. Marion Dufresne, collecting unprecedented data on atmospheric aerosols, greenhouse gases, ultraviolet radiation, and water vapor, along with high-resolution phytoplankton observations in surface waters. The primary objective of MAP-IO is to assess the feasibility of establishing a permanent marine observatory aboard the Marion Dufresne, integrating it into international atmospheric and oceanographic monitoring networks. The collected data provide valuable insights into aerosol distribution and optical thickness, as well as seasonal variability in marine aerosols, greenhouse gases, and ocean-atmosphere interactions in these climatically sensitive regions. MAP-IO represents a strategic initiative to bridge observational gaps, enabling more accurate assessments of regional aerosol dynamics and their climatic impacts while supporting the development and validation of aerosol retrieval algorithms for marine environments, such as those explored in this study. In 2025, MAP-IO was accredited as a French CNRS National Instrument, securing its operation until at least 2030. All observations collected under the MAP-IO program are freely available through the AERIS atmospheric data center (https://www.aeris-data.fr/catalogue-map-io/, last access: 31 May 2025) and the SEANOE ocean data center (https://doi.org/10.17882/89505, last access: 31 May 2025). Further details are available at www.mapio.re (last access: 31 May 2025) and in Tulet et al. (2024).

3 Data Analysis

3.1 Aerosol Optical Depth

This section presents the AOD measurements obtained aboard the R.V. Marion Dufresne over a three-year period, from July 1, 2021, to June 30, 2024. Table 1 summarizes the key statistical metrics for this dataset, including the total number of data points per channel, the mean and standard deviation, and the percentiles at 5%, 25%, 50%, 75%, and 95%, along with the minimum and maximum values.

The total number of measurements containing at least one wavelength at Level 1.5 is $25,602$, including $17,293$ recorded during the day and $7,735$ at night using Moon light. Among the available spectral channels, only 500 and 870 nm are present in all Level 1.5 records. It is important to note that certain Level 1.0 criteria (outlined in subsection 2.2 and detailed in Giles et al., 2019) apply to individual channels and can result in the exclusion of specific wavelengths. Since Level 1.5 processing requires a valid Level 1.0 measurement, any data failing Level 1.0 checks cannot advance to Level 1.5. Furthermore, the transition from Level 1.0 to Level 1.5 most often leads to the rejection of the entire spectral AOD measurement (typically due to general

14

Table 1. Summary statistics of the AOD and α data collected aboard the R.V. Marion Dufresne from July 1, 2021, to June 30, 2024. The table includes the total number of data points for each channel, the mean value and its standard deviation, and percentiles at 5%, 25%, 50%, 75%, and 95%, along with the minimum and maximum values.

Value	Count	Mean	Std	Min	5%	25%	50%	75%	95%	Max
AOD_{340}	17302	0.116	0.118	0.007	0.034	0.059	0.086	0.120	0.308	1.009
AOD_{380}	17314	0.112	0.104	0.012	0.037	0.062	0.085	0.117	0.284	0.888
AOD_{440}	25059	0.093	0.075	-0.005	0.031	0.054	0.075	0.103	0.207	0.717
AOD_{500}	25062	0.084	0.063	0.009	0.030	0.051	0.070	0.095	0.182	0.584
AOD_{675}	25061	0.063	0.041	0.004	0.021	0.039	0.054	0.075	0.136	0.384
AOD_{870}	25062	0.054	0.031	0.003	0.017	0.034	0.048	0.067	0.115	0.328
AOD_{1020}	24995	0.049	0.029	0.001	0.014	0.029	0.043	0.061	0.105	0.341
AOD_{1640}	24765	0.036	0.026	-0.006	0.006	0.019	0.030	0.047	0.082	0.367
α	25062	0.754	0.400	-0.823	0.182	0.459	0.691	1.024	1.484	2.546

cloud-screening criteria, see Subsection 2.2). However, in some cases, Level 1.5 criteria apply only to individual wavelengths[3]. This explains the very few rejections observed in the 440 and 675 nm channels (only 3 and 1 cases, respectively).

405   A significant portion of the missing data in the remaining channels is attributable to nighttime observations, although some exclusions also result from the aforementioned Level 1.0 and Level 1.5 criteria applied to individual wavelengths. For the 340 nm and 380 nm channels, AOD estimation from Moon measurements systematically excludes these wavelengths due to the low incoming lunar irradiance in this spectral range (Barreto et al., 2013, 2016). As a result, none of the 7,735 nighttime Level 1.5 measurements include these two channels. For the near-infrared channels (1020 nm and especially 1640 nm), the

410 lunar irradiance signal is lower than in the visible range. This limitation is particularly pronounced during the first and last quarters of the lunar cycle (the first and last days with AOD night observations), when the received light is minimal. On one hand, this increases the measurement uncertainty for these channels compared to the visible range on these moon quarter days (Barreto et al., 2016). On the other hand, if the signal is too weak, it may fail the Level 1.0 filters related to minimum signal requirements, either due to the minimum digital number threshold or because the signal is lower than the extraterrestrial signal

415 divided by 1500, both of which apply to individual wavelengths. As a consequence, some moon quarter days lack AOD data at 1020 nm and 1640 nm, even when measurements are available for visible channels. This explains most of the nearly 300 missing data points at 1640 nm and the 67 missing at 1020 nm.

Table 2 presents the same statistics as Table 1, but computed using daily mean AOD values. This analysis includes a total of 344 days of observations, of which 60 contain only nighttime measurements, meaning the 340 and 380 nm channels have

420 valid data for 284 days. This results in an overall observation frequency of approximately one out of every three days over the

---

[3]For instance, criteria such as "Aerosol optical depth spectral dependence" and "Large aerosol optical depth triplet variability" (subsections 3.3.5 and 3.3.6 in Giles et al. (2019)) applied specifically to individual wavelengths.

three-year study period, largely due to extended periods when the vessel was not declared on a mission. Figure 3 shows the temporal evolution of these daily means for AOD_{440} and α from July 1, 2021, to June 30, 2024.

The mean AOD values from the full dataset in Table 1 are 0.093 ± 0.075, 0.063 ± 0.041, and 0.054 ± 0.031 at 440, 675, and 870 nm, respectively. These values remain consistent when calculated from daily averages, as shown in Table 2, yielding 0.091 ± 0.067, 0.064 ± 0.038, and 0.056 ± 0.030 for the same three channels. Additionally, the α mean is 0.75 ± 0.40 for the entire dataset and 0.72 ± 0.37 when computed from daily averages. These averages confirm the overall pristine atmospheric conditions in the most common operational area of the R.V. Marion Dufresne, which are characteristic of the southwestern Indian Ocean. These findings are consistent with those reported by Mallet et al. (2018) and other studies conducted in the region (references therein), and they generally align with observations from other clean marine environments with minimal continental influence (Smirnov et al., 2002).

It is important to note that the study includes all AOD measurements recorded aboard the R.V. Marion Dufresne, corresponding to its regular operational area in the southwestern Indian Ocean, including voyages to the French Southern and Antarctic Territories (TAAF), with the sole exception of a short period during the Amaryllis-Amagas and Transama campaigns (April–June 2023), when the vessel traveled from its regular base to the Brazilian coast[4] and back. This segment represents less than 5% of the total dataset. Importantly, the AOD statistics computed exclusively for the Transama transit campaign (AOD_{440} = 0.08 and α = 0.06) are very similar to the global averages, confirming their representativeness and minimal influence on the overall results. Moreover, although the vessel approached the Brazilian coast during Amaryllis-Amagas, no photometer measurements were collected in that area due to the lack of authorization from Brazilian authorities; thus, the available data of that period correspond exclusively to the transit campaign between La Réunion and Brazil, and back.

The general pristine conditions during the three years of measurements on board R.V. Marion Dufresne are clearly observed in Figure 3, where daily averaged AOD_{440} values rarely exceed 0.2, with the vast majority remaining below 0.1 (the 75th percentile limit for both the full dataset and the daily means). It should also be noted that α exhibits a large variability, as reflected in its standard deviation of 0.37 and clearly visible in Figure 3. This variability is in part due to the very low AOD conditions frequently observed in the region. For example, the mean AOD_{870} is 0.056, with a median of 0.05, while the associated uncertainty in AOD retrievals is approximately 0.01 (Eck et al., 1999). This implies that at least 50% of the data in this channel have an uncertainty of at least 20% in the AOD measurement itself, which significantly affects the accuracy of α calculations under such low aerosol load conditions and may explain a large part of the observed variation.

Long-term observations from the AERONET Saint-Denis site provide a valuable reference for assessing aerosol conditions in the most common operational area of the R.V. Marion Dufresne. The data from this site was previously used to contextualize the transition rates between AOD data quality levels for the R.V. Marion Dufresne in subsection 2.2 and will be further utilized in a point-by-point comparison in subsection 3.2.2. For the period 2007–2019, Duflot et al. (2022) reported a mean AOD_{440} of 0.08 and an α of 0.71, values that closely match those obtained in this study (0.09 and 0.72, respectively, from daily averages). According to Duflot et al. (2022), these averages reflect the regional dominance of marine aerosols, providing a representative

---

[4]Further information about these campaigns is available at https://www.ipsl.fr/campagne/amaryllis-amagas/ and https://archimer.ifremer.fr/doc/00875/98738/108483.pdf (last accessed: December 31, 2024).

Table 2. Statistical summary of daily mean AOD and α values at different wavelengths obtained aboard the R.V. Marion Dufresne from July 1, 2021, to June 30, 2024. The table presents the number of valid daily averages per channel, the mean and standard deviation, and percentiles at 5%, 25%, 50%, 75%, and 95%, along with the minimum and maximum values.

Value	Count	Mean	Std	Min	5%	25%	50%	75%	95%	Max
AOD_{340}	284	0.110	0.099	0.015	0.034	0.063	0.089	0.117	0.247	0.809
AOD_{380}	284	0.107	0.087	0.020	0.037	0.067	0.087	0.114	0.227	0.710
AOD_{440}	344	0.091	0.067	0.019	0.032	0.058	0.076	0.098	0.185	0.579
AOD_{500}	344	0.083	0.056	0.015	0.029	0.055	0.072	0.092	0.162	0.478
AOD_{675}	344	0.064	0.038	0.009	0.020	0.042	0.057	0.074	0.128	0.285
AOD_{870}	344	0.056	0.030	0.007	0.017	0.037	0.050	0.067	0.114	0.198
AOD_{1020}	344	0.051	0.028	0.006	0.015	0.033	0.045	0.063	0.105	0.173
AOD_{1640}	344	0.039	0.025	0.000	0.007	0.023	0.034	0.050	0.087	0.156
α	344	0.716	0.371	0.032	0.200	0.426	0.638	0.979	1.397	1.782

baseline for the local atmospheric column. Comparable statistics for the α can be found in Smirnov et al. (2011), whose Figure 5c (MAN climatology from Indian Ocean) shows a similar variation range[5] with a 50% percentile of approximately 0.6, slightly lower than the 0.64 observed in this study for the daily averages (Table 2).

The study by Duflot et al. (2022) highlights the significant seasonal impact of biomass burning emissions, primarily due to bushfires, particularly during the September–October–November (SON) period. During the extended dry season, which spans from late July to early December (shortly before the onset of the first significant rains), emissions from southeastern Africa and Madagascar lead to a substantial increase in AOD and α values, indicating a greater dominance of fine-mode particles in the region. Duflot et al. (2022) notes that while sea salt aerosols are consistently present throughout the year and contribute significantly to AOD, they account for only 16.3% of its variability. In contrast, biomass burning emissions dominate this variability, contributing 67.4%. Thus, sea salt establishes the regional AOD baseline, while biomass burning plumes drive the most significant fluctuations during the dry season.

An extraordinary biomass burning plume was detected aboard the R.V. Marion Dufresne from October 11 to 20, 2023, in the vicinity of La Réunion. As seen in Figure 3, this period stands out as the only one in the entire dataset where daily mean AOD_{440} values exceed 0.3. Notably, 65% of the data within the top 5% percentile of AOD_{440} for the three-year dataset were recorded during this event. Furthermore, all measurements in the top 2.1% percentile (approximately 580 measurements with AOD_{440} exceeding 0.36) occurred between October 12 and 19, 2023. The highest AOD_{440} value recorded in the dataset (0.73,

[5]It is worth noting that while a minimum α value of -0.823 is reported here, less than 0.6% of the data are negative. Similarly, negative values have also been observed in the region by Smirnov et al. (2011). These occurrences are generally associated with very low AOD conditions ($AOD440 < 0.05$), where the relative uncertainty of AOD measurements (estimated at 0.01 for standard channels and 0.02 for UV channels; see Eck et al., 1999) can range from 20% to 100% for AOD_{440}, considering that the minimum observed values are 0.019 for daily means and 0.01 for the full dataset. This uncertainty is even higher for AOD_{870}, where AOD values are generally lower. These large relative errors significantly impact the accuracy of α calculations.
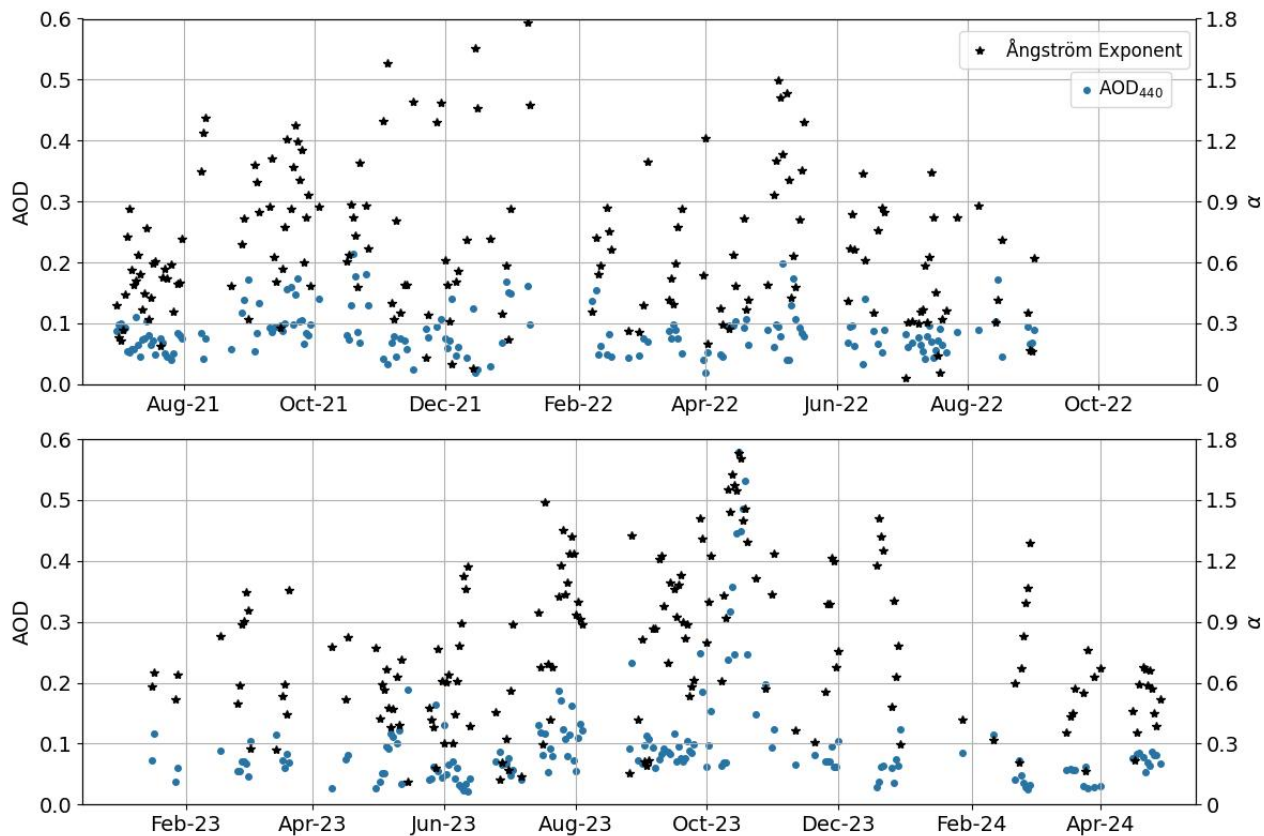
Figure 3. Time series of daily mean AOD Level 1.5 at 440 nm (blue dots) and α values (black asterisks, right y-axis) recorded by the shipborne-adapted CIMEL CE318-T photometer aboard the R.V. Marion Dufresne from July 1, 2021, to June 30, 2024.

see Table 1) and the highest daily average (0.58, see Table 2) both occurred on October 16, 2023. The weekly average AOD_{440} and α reached 0.45 and 1.56, respectively well above the 95th percentile of AOD_{440} (0.21) and α (1.46) for the three-year dataset (Table 1).

While Duflot et al. (2022) acknowledges the presence of biomass burning events in the region and their impact on AOD, their study does not provide a detailed analysis of individual episodes concerning aerosol optical and microphysical properties. Other studies, such as Clain et al. (2009), Duflot et al. (2010), Vigouroux et al. (2012), and Verreyken et al. (2020), primarily focus on the gas-phase contributions associated with individual biomass burning events in the region, without providing insights into aerosol properties. On the other hand, Smirnov et al. (2011) documented a similar episode in the southwest Indian Ocean region on November 12, 2009, where AOD_{500} measured from a vessel reached approximately 0.60 with an α of about 1.4. However, this episode was detected in the Mozambique Channel and likely did not extend to La Réunion, as AOD_{500} values measured at the Saint-Denis site (Level 2) for November 2009 rarely exceeded 0.15, except for a few measurements on November 5.

Additionally, no detailed aerosol retrievals analyzing properties such as size distribution or optical parameters were performed for this event, as Smirnov et al. (2011) relied on MAN data, which lack the sky radiance measurements required for AERONET aerosol retrievals.

Note that sky radiance observations were collected alongside automated AOD measurements aboard the R.V. Marion Dufresne during that week, enabling the retrieval of microphysical and optical aerosol properties using AERONET's standard retrieval algorithm. The exceptionally high AOD values measured during the biomass burning event of October 11–20, 2023, provide a unique opportunity to evaluate the first quality-assured AERONET aerosol retrievals ($AOD_{440} > 0.4$) obtained from a shipborne platform. A detailed analysis of this event and the retrieved optical and microphysical aerosol properties will be presented in Section 4.

3.2   Data validation

As mentioned in the Introduction, an initial validation of AOD data from the shipborne version of the CE318-T photometer was carried out by Yin et al. (2019), who compared automated AOD measurements with a MAN Microtops II instrument aboard the R.V. Polarstern during the OCEANET transatlantic campaigns (PS113, PS116, and MOSAIC/Arctic). However, a similar comparison could not be performed in this study, as no Microtops measurements were conducted aboard the R.V. Marion Dufresne during the three-year period from July 2021 to June 2024. Instead, the present study provides a complementary validation based on a shipborne intercomparison during overlapping operation and on ground-based AERONET data from the nearby Saint-Denis site when the vessel was in proximity.

3.2.1   Validation during the Transama campaign

Throughout the full three-year period of analysis, two different photometers were deployed. The first instrument, labeled #1273, operated from July 1, 2021, until June 12, 2023, when it was scheduled for calibration and replacement. This replacement coincided with the Amaryllis-Amagas and Transama campaigns, during which the vessel was temporarily relocated from its usual operational area in the southwestern Indian Ocean to the Brazilian coast. During the Transama campaign, both the outgoing instrument (#1273) and its replacement, labeled #1243, were kept onboard, allowing for simultaneous operation between April and June 2023. This overlap enabled additional tests and optimizations[6] by research engineers involved in the campaign. For the time series presented in the previous subsection, data from instrument #1273 were used until May 31, 2023, after which data from instrument #1243 were used until June 30, 2024.

Figure 4 presents the comparison of coincident data, using Level 1.5 AOD from both instruments (the highest quality level achievable for moving platform data). This includes AOD measurements at (from top to bottom and left to right) 380, 440, 500, 675, and 870 nm, as well as α. In this analysis, AOD measurements from photometer #1273 (plotted on the x-axis) were

---

[6]For instance, a shorter collimator was tested to reduce wind-induced instabilities, as wind significantly affects data collection at sea. Software modifications were also implemented, and the two photometers were placed in different locations on the vessel to assess the impact of ship vibrations and movement. Elastic lidar measurements were performed in parallel, enabling Klett inversions based on total extinction derived from combined photometer and lidar signals. Further details on remote sensing data and instrumentation from the Amaryllis-Amagas/Transama campaign can be found in Sanchez-Barrero (2024).

compared with AOD values from photometer #1243 (plotted on the y-axis) averaged within a ± 3 minute interval. All AOD datasets include 1180 data points, except for the 380 nm channel which is limited to 622 points since AOD_{380} is provided only during daytime (Moon-based AOD measurements do not include this wavelength, as explained in subsection 2.2). The α comparison is also based on 1180 points. Color bars represent data density, using a 0.01×0.01 grid for AOD comparisons and a 0.1×0.1 grid for α. A logarithmic scale was applied to the density representation to better visualize the high concentration of data points along the one-to-one line.

As shown in the panels, the agreement between the two instruments is particularly strong, with R exceeding 0.96 for all AOD channels and slopes ranging from 0.92 to 0.98. The corresponding RMSE values lie between 0.005 to 0.008, which are slightly lower than those reported by Yin et al. (2019), where differences relative to the Microtops-II instrument ranged from 0.009 to 0.015 (see Figure 4 in their study). In addition, the biases, computed as AOD(#1273) - AOD(#1243), are also minimal, with values of 4.2×10^{-3}, -1.7×10^{-3}, -8.0×10^{-5}, 1.6×10^{-3}, and 2.0×10^{-3} for the 380, 440, 500, 675, and 870 nm channels, respectively. These biases are slightly smaller than those reported in Yin et al. (2019), where they ranged from 2×10^{-3} to 5×10^{-3}. Notably, the high correlations and low biases observed for AOD comparison in this study are comparable to those obtained in ground-based calibration sites during intercalibration periods with AERONET master instruments (Holben et al., 1998), demonstrating the reliability of shipborne Level 1.5 data.

However, the comparison for α shows a much higher RMSE (0.158 vs. 0.063) and a slightly lower correlation (R = 0.73 vs. 0.9) than those reported by Yin et al. (2019). These larger discrepancies for α, despite smaller differences in AOD, might be attributed to the significantly low AOD values observed during the Amaryllis-Amagas/Transama campaign, which took place under pristine conditions (with AOD_{440} below 0.18, except for one night with measurements reaching up to 0.27), in contrast to the higher values reported by Yin et al. (2019), where AOD_{440} reached up to 0.6. As mentioned in the previous section, when AOD values are low, the relative errors tend to be much larger, which has a more pronounced impact on α. For instance, if the analysis is restricted to cases where $\text{AOD}_{870} > 0.05$ (not shown in any figure, with 490 data points), the RMSE for α decreases to 0.12, and the correlation coefficient increases to 0.8.

3.2.2 Validation against AERONET Saint-Denis observations

An additional validation of the shipborne CE318-T is conducted using the AERONET ground-based photometer at the Saint-Denis site, previously introduced in subsection 3.1. Located 93 meters above sea level and approximately 20 km from the port of La Réunion, this site offers a unique opportunity for comparison due to the frequent proximity of the R.V. Marion Dufresne during its regular entries and departures. As the nearest ground-based AERONET site with the highest number of coincident measurements, it serves as a key validation point for the shipborne data, despite the inherent challenges posed by the elevation difference.

Figure 5 presents the correlation between AOD and α data from the CE318-T at the Saint-Denis AERONET site and the shipborne photometer aboard the R.V. Marion Dufresne. These comparisons were conducted over the full three-year period of data collection. To ensure meaningful comparisons, measurements were selected when the R.V. Marion Dufresne was within a maximum distance of 50 km from the Saint-Denis site. Notably, adjusting the threshold between 30 and 100 km had only a
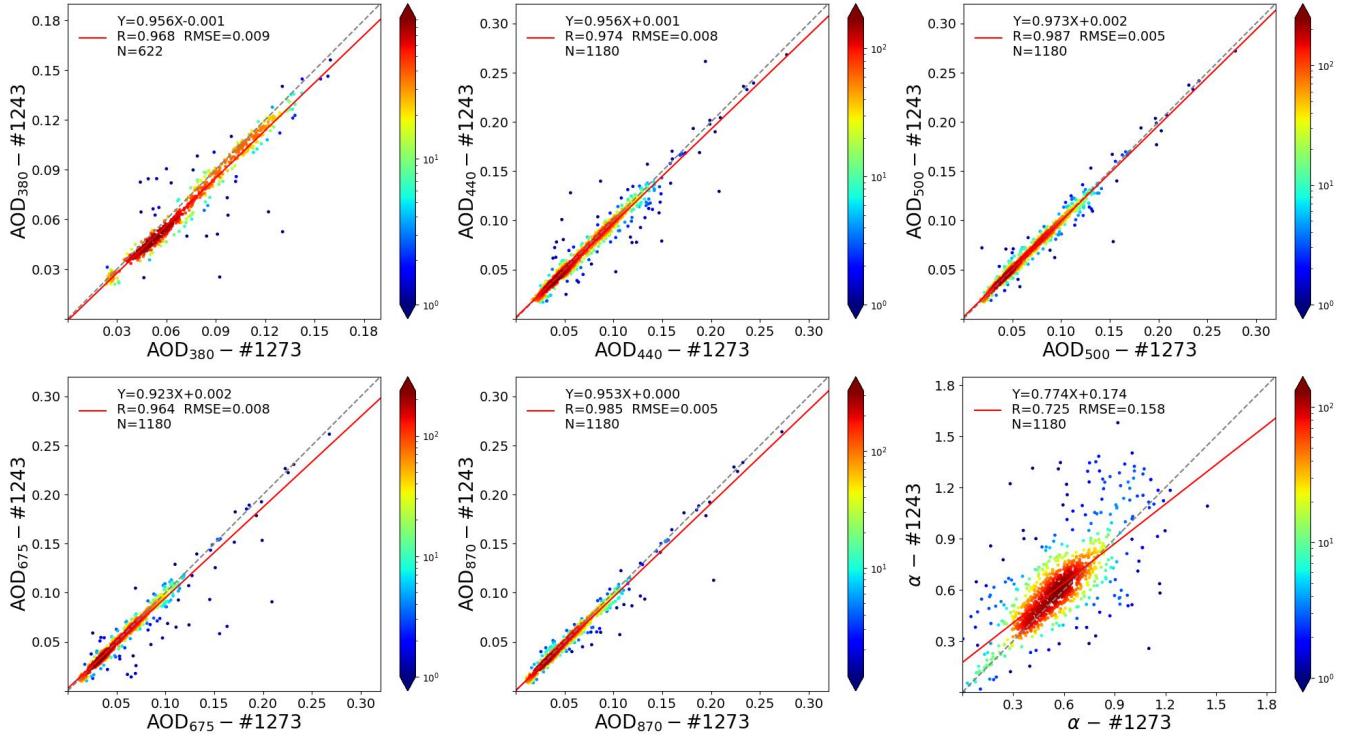
Figure 4. Comparison of Level 1.5 AOD and α measurements between photometer #1273 (x-axis) and photometer #1243 (y-axis) during the Amaryllis-Amagas/Transama campaign from late April to early June 2023. The comparison is shown for the AOD channels 380, 440, 500, 675, and 870 nm (top to bottom, left to right) and the α. Color bars represent data density on a 0.01×0.01 grid for AOD and a 0.1×0.1 grid for α, with a logarithmic scale applied due to the high data density along the one-to-one line. For each AOD measurement from photometer #1273, the comparison was made with the average of AOD data from photometer #1243 within a ± 3-minute interval. All data shown have undergone the Level 1.5 cloud-screening and quality control procedures described in subsection 2.2 and references therein.

minor impact on the dataset size, with 1745 points at 30 km, 1833 points at 50 km (the selected threshold), and 1941 points at 100 km. The statistical results (e.g., RMSE, slopes, and correlation coefficients) remained largely unchanged across these thresholds. However, a significant reduction occurs when using a stricter 20 km limit, leaving only 8 coincident observations. This sharp drop is explained by the fact that the distance between the ship's docking location in Le Port and the Saint-Denis photometer is approximately 21 km, meaning that most entries and departures fall just outside the 20 km range.

For each comparison, the shipborne data were averaged over a ± 3-minute interval relative to the ground-based measurements. The figure follows the same structure as Figure 4, displaying AOD comparisons at 380, 440, 500, 675, and 870 nm, along with α (arranged top to bottom, left to right). To ensure the highest data quality, only Level 2 AERONET data from Saint-Denis were used in this comparison. Since Moon-based AERONET observations are still under evaluation and have not yet reached Level 2 status, the comparison includes only AOD values obtained from direct Sun measurements.
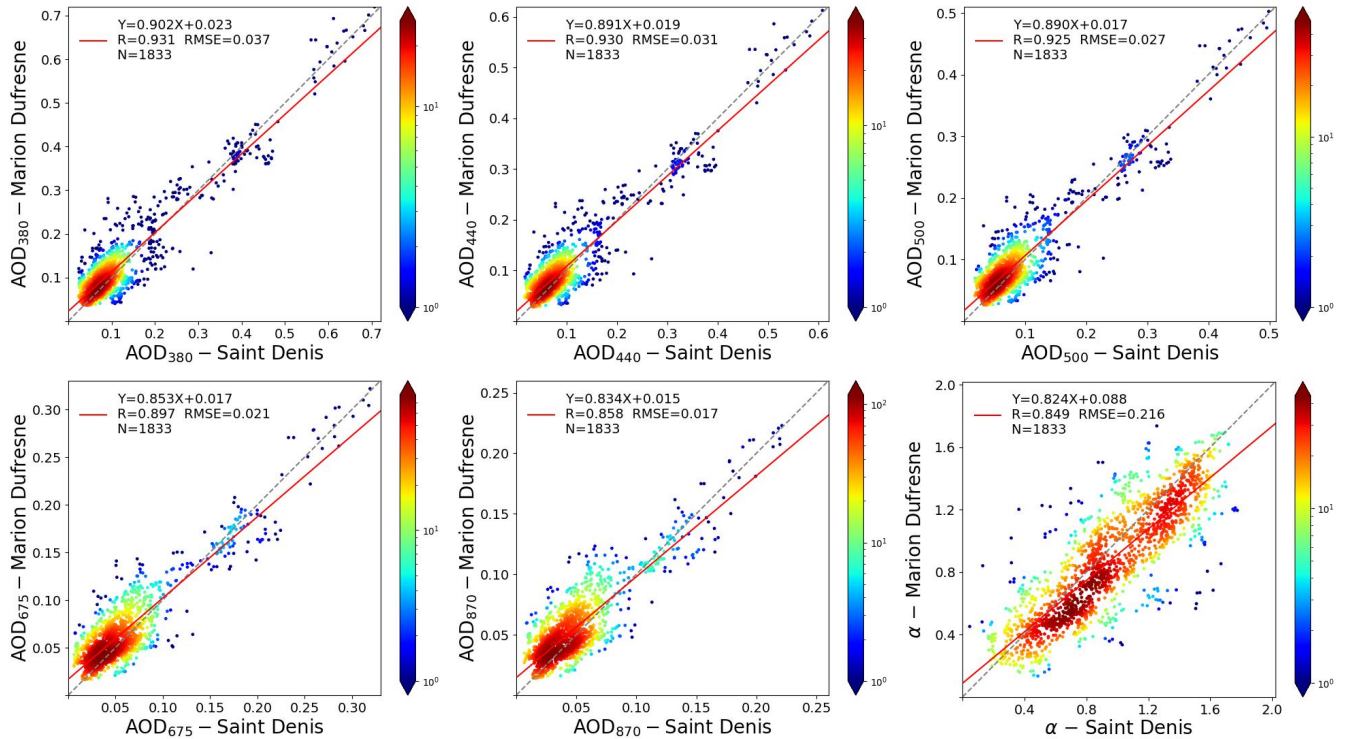
Figure 5. Comparison of AOD and α measurements between the ground-based photometer at Saint-Denis (x-axis) and the shipborne photometer aboard the R.V. Marion Dufresne (y-axis). The comparison is shown for the AOD channels 380, 440, 500, 675, and 870 nm (top to bottom, left to right) and α. Color bars represent data density on a 0.01×0.01 grid for AOD and a 0.1×0.1 grid for α, with a logarithmic scale used due to strong data density along the one-to-one line. For each AOD measurement from the R.V. Marion Dufresne, the comparison was made with the average of AOD data from the Saint-Denis photometer within a ± 3-minute interval, and only when the ship was within a maximum distance of 50 km from the Saint-Denis site.

The correlations between the shipborne and ground-based photometers are generally strong, with R values ranging from 555 0.86 to 0.93. However, a clear negative bias is observed when using the Saint-Denis photometer as a reference. The bias values are -1.3×10^{-2}, -9.5×10^{-3}, -8.7×10^{-3}, -8.8×10^{-3}, and -7.0×10^{-3} for the 380, 440, 500, 675, and 870 nm channels, respectively. These biases are approximately an order of magnitude larger than those found in the previous instrument intercomparison, likely due to the altitude difference between the Saint-Denis station (93 m above sea level) and sea level. Additionally, notable differences in local pollution levels may contribute to these discrepancies. While Saint-Denis is a relatively 560 cleaner urban site, the R.V. Marion Dufresne is often docked in Le Port, an area heavily influenced by industrial emissions, including those from a coal-fired power plant.

Upon examining the RMSE values between the shipborne and ground-based photometers, it is noted that they are approximately double the typical AERONET error estimates for the respective wavelengths. Specifically, the RMSE values are 0.037, 0.031, 0.027, 0.021, and 0.017 for the 380, 440, 500, 675, and 870 nm channels, respectively (AERONET error estimates are

around 0.02 for the 380 nm channel and 0.01 for the channels 675 and 870 nm, for 440 and 500 nm an intermediate value of 0.015 can be expected Eck et al., 1999). Despite these higher RMSE values, the agreement between the shipborne and ground-based measurements remains within acceptable limits. Even if the altitude difference were not considered, the comparison between the two instruments would still be reasonable.

There is also a positive bias for α of 0.08. The larger values at the Saint-Denis site could be attributed to a diminished influence of marine aerosols and a relatively greater contribution from local urban aerosols in the city, primarily consisting of smaller particles, as reported by Duflot et al. (2022). Nevertheless, a relatively strong correlation for α is observed, better than that seen in Figure 4, indicating that both instruments are identifying similar aerosol types in the atmospheric column, with the primary difference being the lowest 93 meters, which may lead to the observed bias in AOD and α measurements. The greater variability of α during the three years analyzed in this study, compared to the Amaryllis-Amagas/Transama campaign, also positively contributes to the improved R values.

4   First quality-assured shipborne AERONET aerosol retrievals of optical and microphysical properties

The use of the modified CE318-T photometer for shipborne platforms has enabled the acquisition of sky radiance measurements, a necessary input for performing aerosol retrievals with the AERONET aerosol algorithm. As introduced in subsection 2.2.4, this algorithm retrieves detailed binned aerosol volume size distributions and spectrally independent optical properties, including refractive index as a primary parameter and derived properties such as SSA and absorption (Dubovik and King, 2000). The systematic collection of sky radiances over the past three years as part of the MAP-IO program aboard the R.V. Marion Dufresne represents a significant milestone, marking the first AERONET aerosol inversions conducted on a shipborne platform.

Among the potential retrievals available from the three-year dataset, those from the week of October 12 to October 19, 2023, stand out as particularly noteworthy. As discussed in Section 3.1, this period corresponds to an extraordinary biomass burning event linked to intense bushfires in Madagascar, which significantly elevated aerosol levels in the surrounding region. Madagascar's bushfire season, which typically spans the dry season from late July to early December (Clain et al., 2009; Duflot et al., 2010, 2022; Vigouroux et al., 2012; Verreyken et al., 2020) as in the rest of southern Africa area, reached a peak in mid-October 2023. During this time, fire alerts were exceptionally high, with the most intense activity concentrated in the western regions of Madagascar. According to the Global Disaster Alert and Coordination System (GDACS), approximately 5,154 hectares were burned during this period. The rigorous criteria required for AERONET Level 2 aerosol optical inversion properties[7] —$AOD_{440} > 0.4$ and $\theta_S > 50°$ (Dubovik et al., 2000; Holben et al., 2006)— were met several times during this period, allowing for the first detailed analysis of retrievals from shipborne measurements under sufficient aerosol load. The results of these retrievals are presented in this section.

---

[7]It is worth noting that the Level 2 criteria for size distribution properties are less stringent, as they do not impose an AOD_{440} threshold. However, they share the remaining conditions with the optical property criteria, such as $\theta_S > 50°$ and a minimum symmetrical number of radiance measurements in the almucantar (or, more recently, in hybrid scans) across different scattering angle ranges, among other. For further details, refer to Table 3 in Holben et al. (2006).
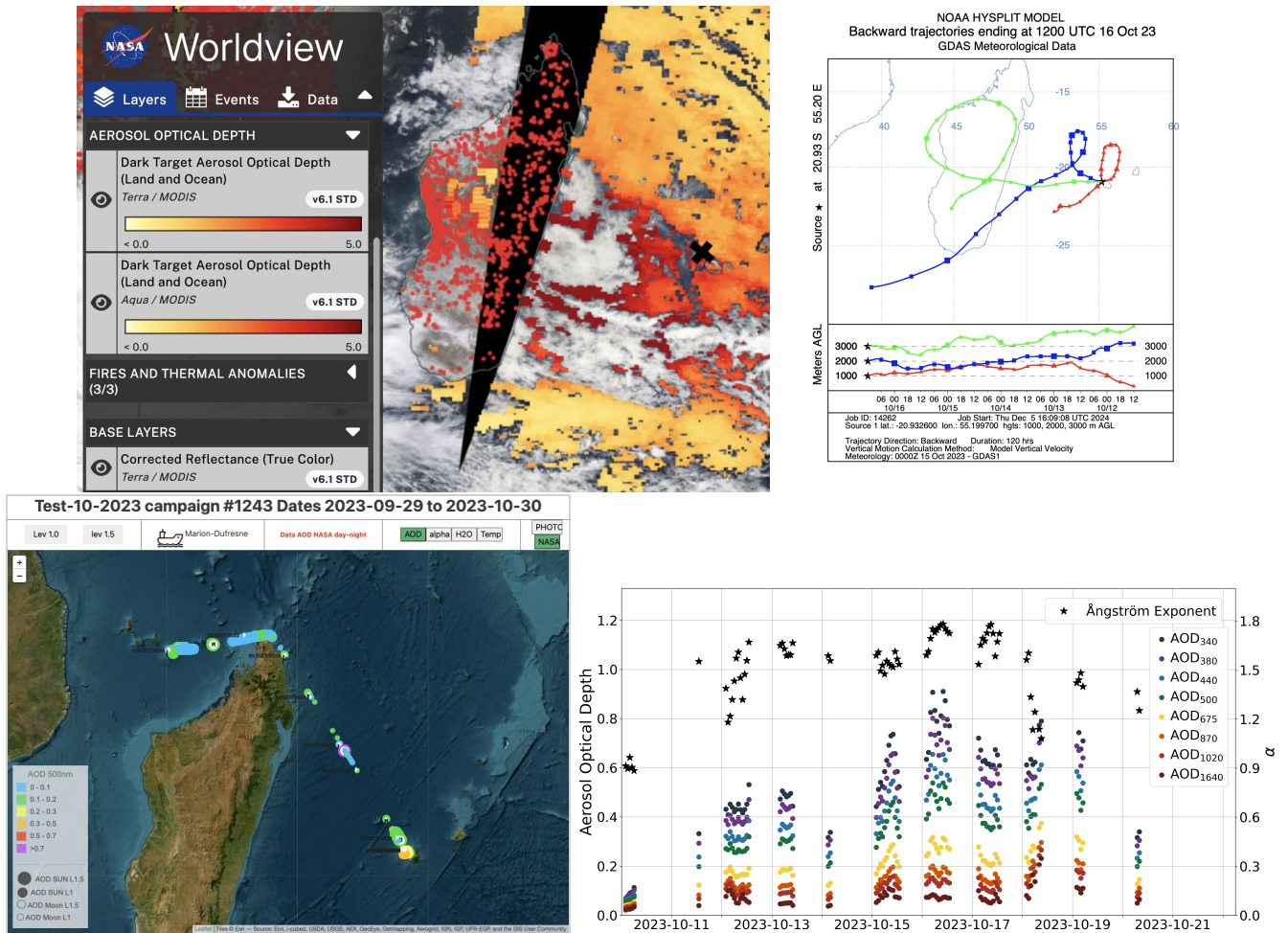
Figure 6. Overview of the aerosol and fire conditions around La Réunion during the week of October 12–19, 2023. Top-left panel: Composite image obtained from NASA Worldview, combining MODIS RGB imagery with the AOD_{550} from October 16 (C6.1 MODIS Dark Target algorithm), overlaid with fire counts detection. The black cross marks the position of the R.V. Marion Dufresne on October 16 (20.93 E, 55.20 S), approximately 12 km northwest of the closest coastal point of La Réunion and 30 km from Saint-Denis. Top-right panel: Backward air mass trajectories for October 16, calculated using the HYSPLIT model. Bottom-left panel: AOD values recorded during the test in the sea area campaign (September 29 to October 30, 2023). Bottom-right panel: Time series of hourly-averaged spectral AOD (Level 1.5) values from October 10 to October 21, represented by navy blue (340 nm), violet (380 nm), light blue (440 nm), green (500 nm), yellow (675 nm), orange (870 nm), red (1020 nm), and brown (1640 nm) dots. Values of α are shown with black asterisks (right y-axis).

The top-left panel of Figure 6 illustrates the aerosol and fire activity around La Réunion during this exceptional week. This composite image, obtained from NASA Worldview, overlays a MODIS RGB image with the AOD product at 550 nm from

24

October 16, derived using the C6.1 MODIS Dark Target (DT) algorithm. The DT algorithm, akin to the Collection 6 version described by Levy et al. (2013), incorporates updates such as enhanced sensor calibration, stricter cloud screening, and an improved surface reflectance model for urban areas (Gupta et al., 2016). The fire counts layer, based on the detection algorithm by Giglio et al. (2003) and depicted as red spots, underscores the widespread distribution of fires across Madagascar during this period. The position of the R.V. Marion Dufresne on October 16, 2023, at 12:11 UTC, is marked with a black cross (20.93°S, 55.20°E) in the figure. This moment represents the first almucantar measurement meeting Level 2 aerosol retrieval criteria[8], not only during this event but also across the entire dataset recorded aboard the R.V. Marion Dufresne since 2021. At this location, the vessel was approximately 12 km northwest of the nearest coastal point of La Réunion and 30 km from the AERONET station in Saint-Denis. The top-right panel of Figure 6 displays back-trajectories, calculated using the HYSPLIT model (Stein et al., 2015), that estimate the origins of the air masses over the R.V. Marion Dufresne on October 16, 2023, at 12:00 UTC, around the time of the almucantar measurement from the boat. At 3000 meters, the air mass forms a loop around Madagascar, traveling counterclockwise from the southwest to the northwest before exiting to the east. At 2000 meters, the air mass crosses the southern part of the island, while at 1000 meters, it remains localized near La Réunion, indicating recirculation and certainly more affected by marine aerosols. These trajectories, calculated over a five-day period with a point every six hours, confirm that the air masses influencing the aerosol observations over the ship predominantly originated from Madagascar, where the biomass burning episode occurred.

The bottom-left panel of Figure 6 illustrates the AOD_{500} recorded between September 29 and October 30, 2023, during the campaign referred to as test in the sea area. These geolocated AOD measurements reveal the ship's trajectory, showing a voyage to northern Madagascar at the beginning of October, characterized by typically pristine AOD values, and shorter trips of two to three days around the port of Saint-Denis from mid-October until the end of the month. Some of these shorter trips coincided with the biomass burning episode. These AOD data are available on the PHOTONS system platform (https: //mobile.photons.univ-lille.fr/, last access: 31 May 2025), and the figure can be directly generated from the web by selecting the R.V. Marion Dufresne and the campaign "2023 MAP-IO Test en mer 2023-10."

The bottom-right panel presents multi-spectral Level 1.5 AOD data recorded by the shipborne-adapted CE318-T photometer from October 10 to October 21, covering the week of interest. The values are displayed as hourly averages for all standard AERONET channels: 340 nm (navy blue dots), 380 nm (violet dots), 440 nm (light blue dots), 500 nm (green dots), 675 nm (yellow dots), 870 nm (orange dots), 1020 nm (red dots) and 1640 nm (brown dots). The temporal evolution of α is represented by black asterisks (right y-axis and also displayed as hourly averages). On October 10, conditions reflect the typical pristine marine environment, dominated by sea salt aerosols, observed during the three-year analysis period. The mean AOD_{440} for this day was 0.076, with an α of 0.88—values consistent with the dataset's overall mean. However, due to abundant cloud cover

---

[8]In this study, retrievals meeting the thresholds of $AOD_{440} > 0.4$ and $\theta_S > 50°$ are referred to as Level 2 to distinguish them from those that do not meet these thresholds. However, official Level 2 status requires that the underlying AOD data be validated and reclassified to Level 2 within the AERONET network. Shipborne measurements are currently classified as Level 1.5, and retrievals satisfying these additional criteria will only be officially recognized as Level 2 once the AOD data are upgraded. Retrievals failing to meet these thresholds will remain classified as Level 1.5 even after reclassification.

during this period (see Figure 6), no data were recorded in the afternoon on October 10, and only limited measurements were obtained on October 11, primarily in the late afternoon.

Starting on October 11, a gradual increase in AOD values, indicative of rising aerosol load, and α values, reflecting fine-mode particle dominance, becomes evident around La Réunion. The values during this period, as already introduced in subsection 3.1, correspond to the most extreme aerosol event of the three-year dataset, with AOD_{440} values consistently exceeding 0.36 and a weekly average of 0.45. The α values during this episode also peaked, averaging 1.56 for the week, well above the 95th percentile of the full dataset. Notably, October 16 registered the highest AOD levels of the entire period, with a shipborne AOD_{500} of 0.49 ± 0.05 around midday, closely matching the MODIS AOD_{550} value of 0.52 observed in Figure 6. After October 19, AOD values gradually declined, with limited measurements on October 20 reflecting this reduction. Persistent cloud cover prevented further AOD data collection until October 31, except for a few observations during the night of October 24. By October 31, atmospheric conditions had returned to a typical clean marine state, with a daily average AOD_{440} of 0.096 and an α of 1.02, consistent with baseline marine aerosol conditions. It should be noted that the marked days in the graph correspond to 00:00 UTC. Due to the geographic location and time of the year, the first morning direct Sun measurements (daylight AOD) began around 2:30 a.m. UTC, provided cloud conditions allowed. Additionally, the new moon occurred on the night of October 14 to October 15, 2023, preventing moon-based AOD measurements during the period from October 8 to 21 (from the last quarter to the first quarter of the lunar phase).

Figures 7 and 8 present the aerosol inversions performed at the R.V. Marion Dufresne and Saint-Denis sites during the week of October 12–19, 2023. The inversions from October 12 are shown separately in Figure 7, as it is the only day with simultaneous measurements from both sites. Figure 8 includes the remaining inversions, consisting of data from the R.V. Marion Dufresne on October 16 and 17, and from Saint-Denis site on October 19. Due to persistent cloud cover during this period, complete inversions were only obtained at Saint-Denis on October 12 and 19, and aboard the R.V. Marion Dufresne on October 12, 16, and 17. In each figure, the panels from left to right represent the volume size distribution, the real part of the refractive index (RRI), and the SSA. The retrievals from the R.V. Marion Dufresne are represented by solid lines, while those from Saint-Denis are shown as dashed lines. The legend in each figure includes the type of scan, the exact date and time of the radiance measurement corresponding to the inversion, θ_S and the AOD_{440}.

Additionally, Table 3 provides a summary of the key parameters derived from the inversions during this period. The first columns of the table include information similar to the figure legends: site name, date, type of scan, θ_S, α and AOD_{440}. The table further presents a concise overview of the aerosol size distribution parameters for both fine and coarse modes, including modal radius (R_{Vf} and R_{Vc} in $[\mu m]$) and volume concentration (C_{Vf} and C_{Vc} in $[\mu m^3/\mu m^2]$). The total effective radius (R_{eff} in $[\mu m]$) is also included. It is important to highlight that these size distribution parameters are derived systematically from the detailed 22-bin size distribution provided by the retrieval algorithm, rather than being direct outputs. Additional details on the methodology to obtain these size parameters can be found in the AERONET inversion product documentation (http://aeronet. gsfc.nasa.gov/new_web/Documents/Inversion_products_V2.pdf, last access: 31 May 2025). Finally, the table summarizes key aerosol optical properties, such as the RRI and the SSA at 440 nm (RRI_{440} and SSA_{440}), offering a comprehensive view of some optical aerosol properties observed during this period.
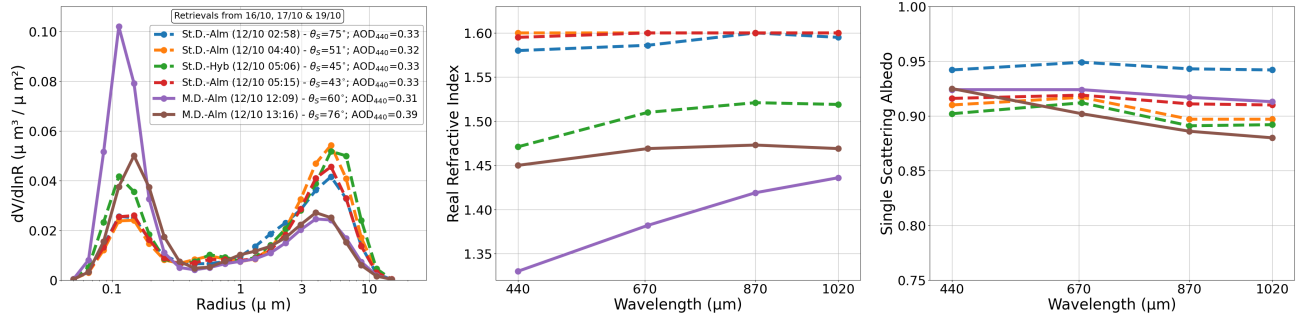
Figure 7. Aerosol retrievals performed on October 12, 2023, at the R.V. Marion Dufresne (solid lines) and Saint-Denis (dashed lines). Panels, from left to right, represent the retrieved 22 bin volume size distribution, the RRI and the SSA at 440, 675, 870 and 1020 nm. The inversions include morning measurements from Saint-Denis and afternoon measurements from the R.V. Marion Dufresne. The legend specifies the type of scan, exact time of radiance measurement, the θ_S and AOD_{440}.
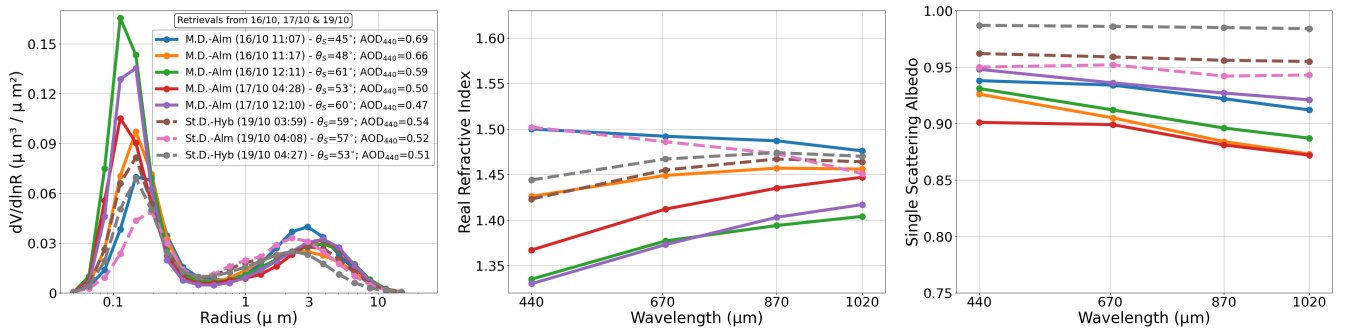

Figure 8. Aerosol retrievals performed at the R.V. Marion Dufresne (October 16 and 17) and Saint-Denis (October 19), 2023. Panels, from left to right, display the retrieved 22 bin volume size distribution, the RRI and the SSA at 440, 675, 870 and 1020 nm. Retrievals from the R.V. Marion Dufresne are shown as solid lines, while those from Saint-Denis are represented as dashed lines. The legend indicates the type of scan, measurement time, θ_S and AOD_{440}.

The inversions from October 12, shown in Figure 7, include morning measurements from the Saint-Denis site and afternoon measurements from the R.V. Marion Dufresne. Due to cloud cover, no valid inversions were obtained from Saint-Denis in the afternoon or from the R.V. Marion Dufresne in the morning. During this day, the R.V. Marion Dufresne was located in the port area of La Réunion, approximately 30 km from the Saint-Denis site. AOD_{440} values remained relatively constant throughout the day, approximately 0.32–0.33, except for the last inversion from the R.V. Marion Dufresne, which recorded a higher value of 0.39. This evolution is also reflected in the R.V. Marion Dufresne measurements presented in Figure 6. Value of α show a more noticeable evolution, increasing from 1.2–1.3 in the morning to 1.5–1.6 in the afternoon (values presented in Table 3 individually for each retrieval). This shift suggests a greater dominance of fine-mode aerosols (biomass burning) over coarse-

27

Table 3. Summary of aerosol inversion parameters obtained at the R.V. Marion Dufresne and Saint-Denis sites during the week of October 12–19, 2023. The table includes the site, date, scan type (almucantar or hybrid), θ_S, α, AOD$_{440}$, size distribution parameters for fine and coarse modes (modal radius R$_{Vf}$ and R$_{Vc}$ in $[\mu m]$ and volume concentration C$_{Vf}$ and C$_{Vc}$ in $[\mu m^3/\mu m^2]$), the total effective radius (R$_{eff}$ in $[\mu m]$), and optical properties including RRI$_{440}$ and SSA$_{440}$

Site	Date	SkyScan	θ_S	AOD$_{440}$	α	R$_{Vf}$	C$_{Vf}$	R$_{Vc}$	C$_{Vc}$	R$_{eff}$	RRI$_{440}$	SSA$_{440}$
St.Denis	12/10 02:58	Alm	75°	0.33	1.40	0.15	0.028	3.11	0.065	0.40	1.58	0.94
St.Denis	12/10 04:40	Alm	51°	0.32	1.25	0.15	0.026	3.30	0.075	0.45	1.60	0.91
St.Denis	12/10 05:06	Hyb	45°	0.33	1.32	0.14	0.044	4.33	0.070	0.37	1.47	0.90
St.Denis	12/10 05:15	Alm	43°	0.33	1.34	0.15	0.028	3.22	0.063	0.41	1.59	0.92
Mar.Dufr.	12/10 12:09	Alm	60°	0.31	1.52	0.13	0.079	2.91	0.041	0.18	1.33	0.92
Mar.Dufr.	12/10 13:16	Alm	76°	0.39	1.65	0.16	0.047	2.71	0.045	0.26	1.45	0.92
Mar.Dufr.	16/10 11:07	Alm	45°	0.69	1.74	0.18	0.070	2.64	0.061	0.28	1.50	0.94
Mar.Dufr.	16/10 11:17	Alm	48°	0.66	1.73	0.16	0.089	2.50	0.049	0.22	1.43	0.93
Mar.Dufr.	16/10 12:11	Alm	61°	0.59	1.72	0.14	0.139	2.81	0.052	0.17	1.33	0.93
Mar.Dufr.	17/10 04:28	Alm	53°	0.50	1.65	0.14	0.094	2.76	0.051	0.19	1.37	0.90
Mar.Dufr.	17/10 12:10	Alm	60°	0.47	1.65	0.14	0.112	2.90	0.052	0.19	1.33	0.95
St.Denis	19/10 03:59	Hyb	59°	0.54	1.49	0.15	0.071	2.20	0.058	0.24	1.42	0.96
St.Denis	19/10 04:08	Alm	57°	0.52	1.51	0.18	0.048	2.08	0.063	0.34	1.50	0.95
St.Denis	19/10 04:27	Hyb	53°	0.51	1.53	0.16	0.066	1.95	0.048	0.24	1.44	0.99

mode aerosols (pristine marine aerosol) as the day progresses. This evolution in α could explain why coarse-mode aerosols are more prominent in the Saint-Denis inversions compared to those from the R.V. Marion Dufresne in the left panel of Figure 7. This trend is further supported by the values of R$_{eff}$ presented in Table 3, where the morning inversions from Saint-Denis range between 0.37–0.45 μm, while the afternoon inversions from the R.V. Marion Dufresne fall between 0.18–0.25μm.

Regarding fine-mode aerosols, while the modal median radius (R$_{Vf}$) remains consistent across inversions from both sites throughout the day (ranging from 0.13 to 0.16 μm), significant differences are observed in concentration values. Notably, higher fine-mode volume concentration values (C$_{Vf}$) are retrieved from the shipborne data (top-right panel, ranging from 0.047 to 0.079 $\mu m^3/\mu m^2$) compared to those obtained at Saint-Denis (ranging from 0.026 to 0.044 $\mu m^3/\mu m^2$). Additionally, lower RRI values are retrieved from the R.V. Marion Dufresne inversions compared to Saint-Denis retrievals. The Saint-Denis inversions at 02:58, 04:40, and 05:15 UTC exhibit C$_{Vf}$ values that are likely underestimated, accompanied by saturated RRI values reaching the upper limit of 1.6. Conversely, the R.V. Marion Dufresne inversion at 12:09 UTC reveals exceptionally high C$_{Vf}$ values and an RRI nearing the lower limit of 1.33 of AERONET inversion for the 440 nm channel. These results are likely due to the well-documented anti-correlation often observed between RRI and fine-mode size distribution, particularly in fine-mode concentration. This phenomenon is extensively described in the literature (Dubovik et al., 2000, 2002b; Torres et al., 2014; Fedarenka et al., 2016; Sinyuk et al., 2020; Herrera et al., 2022). For instance, Figure 33 of Herrera et al. (2022) illustrates the correlation matrix for retrieval unknowns in a simulated biomass burning scenario, revealing a strong negative

correlation (dark blue) between RRI and fine-mode size distribution concentrations. The absence of angular measurements in some scenarios, particularly between $40°$ and $90°$ of scattering angle due to cloud screening criteria in almucantar and hybrid scans based on symmetry tests, likely amplifies this anti-correlation in the dataset from both sites during that week. It is worth noting that polarimetric observations can mitigate this anti-correlation and improve retrieval accuracy, as shown in sensitivity studies by Fedarenka et al. (2016). However, neither the shipborne nor the Saint-Denis photometers were equipped with calibrated polarized measurement, limiting further exploration of this issue.

Two inversions—Saint-Denis at 05:06 UTC and R.V. Marion Dufresne at 13:16 UTC—show intermediate and similar values for both the size distribution and RRI, making them the most realistic representations of the columnar aerosol properties for this day. These intermediate RRI values, ranging from 1.45 to 1.52, are reasonably expected for a mix of biomass burning and sea salt aerosols. While Dubovik et al. (2002b) reported an RRI of approximately 1.51 for pure biomass burning aerosols in southern Africa, the mixture with sea salt could reduce the RRI since the value of this aerosol component is typically between 1.35 and 1.40, depending on water uptake of sea salt under high relative humidity conditions (Schuster et al., 2009). It is important to highlight that there are no detailed studies available for direct comparison of the observed columnar RRI values in this specific region, including the south-eastern African Indian Ocean and the Madagascar-La Réunion area, where, under high aerosol load conditions, biomass burning is typically mixed with sea salt aerosols (Duflot et al., 2022). Although many studies have investigated the gas phase contributions associated with biomass burning episodes in the region (Clain et al., 2009; Duflot et al., 2010; Vigouroux et al., 2012; Verreyken et al., 2020) and Duflot et al. (2022) provided some insights into aerosol size properties, detailed analyses of column-integrated aerosol optical properties remain scarce - mainly due to the very limited availability of Level 2 aerosol inversions in this region. At the Saint-Denis site, for instance, only nine almucantar inversions meet the Level 2 criteria of $AOD_{440} > 0.4$ and $\theta_S > 50°$ across the entire dataset (2003–2024). These inversions are exclusively from the dry season and likely represent a mixture of biomass burning and sea salt aerosols (Duflot et al., 2022). The average RRI values for these nine inversions at Saint-Denis are 1.51 ± 0.06, 1.49 ± 0.05, 1.48 ± 0.05, and 1.46 ± 0.05 at 440, 670, 870, and 1020 nm, respectively, and are similar to the intermediate values found in the two aforementioned inversions. The relatively high variability (standard deviation) in these RRI values is likely driven primarily by varying contributions of sea salt aerosols in the mixture, which can lower the RRI compared to that of pure biomass burning aerosols. Another potential contributor to this variability is the previously mentioned anti-correlation, which introduces a relatively high uncertainty in the RRI values derived from AERONET inversions. For reference, Sinyuk et al. (2020) reported an uncertainty of approximately 0.02 in RRI for pure African biomass burning aerosols when $AOD_{440} = 0.4$.

As noted by Sinyuk et al. (2020), despite the anti-correlation between RRI and fine-mode aerosol volume concentration, their combined effects counterbalance in terms of aerosol scattering. Thus, the capability of AERONET-type inversions to accurately distinguish between absorption and scattering remains unaffected, even in cases where the anti-correlation is significant. Consequently, even in scenarios with high uncertainties in RRI and fine-mode volume concentration, the retrieval of SSA is highly accurate under the conditions established by Level 2 retrieval criteria. The SSA values observed in the shipborne and Saint-Denis inversions (right panel) are therefore reliable and show spectral values ranging from 0.88 to 0.95, with most falling between 0.90 and 0.92. These values are less absorbing than the averages typically found in pure biomass burning

episodes in southern Africa (e.g. Dubovik et al., 2002a; Giles et al., 2012; Denjean et al., 2020), which range between 0.75 and 0.85. The higher SSA values observed here are consistent with what is expected for a case of mixed biomass burning and sea salt aerosols—a highly scattering and non-absorbing aerosol type—or, more generally, even for aging biomass burning aerosols influenced by high relative humidity (Mallet et al., 2019). Indeed, the spectral SSA averages of the aforementioned nine AERONET Level 2 inversions from Saint Denis are 0.92 ± 0.03, 0.89 ± 0.03, 0.87 ± 0.04, and 0.85 ± 0.04 at 440, 670, 870, and 1020 nm, respectively. The SSA values retrieved from the inversions presented in Figure 7 are broadly consistent with these averages, though they appear slightly less absorbing overall. Among them, the inversion from the R.V. Marion Dufresne at 13:16 UTC stands out as the closest match to the Level 2 averages at Saint-Denis site, with spectral SSA values of 0.92, 0.90, 0.89, and 0.88 at 440, 670, 870, and 1020 nm, respectively. This retrieval, with an AOD_{440} of 0.39 and $\theta_S = 75.8°$, is the only one on October 12 that nearly satisfies Level 2 criteria, further supporting the reliability of shipborne retrievals under conditions of sufficient aerosol load.

Beyond the retrievals performed on October 12, additional inversions were obtained from the R.V. Marion Dufresne on October 16 and 17, and from the Saint-Denis site on October 19, as shown in Figure 8. The lack of coincident retrievals between the two sites on these dates is primarily attributed to persistent cloud cover in the region, which limited the number of valid sky radiance measurements. Although the inversions from Saint-Denis on October 19 satisfy the $AOD_{440} > 0.4$ and $\theta_S > 50°$ criteria (including two hybrid and one almucantar scans), they do not achieve Level 2 status due to insufficient valid radiances under the symmetry criteria, likely a consequence of the prevalent cloud cover (Level 2 inversions require more valid radiance angles than Level 1.5, for more details see Table 3 from Holben et al., 2006). For the retrievals from the R.V. Marion Dufresne, R_{Vf} values ranging between 0.14 and 0.18 μm and R_{eff} values between 0.19 and 0.28 μm are consistent across the inversions, align with the values observed on October 12, and agree with the retrievals from Saint-Denis on October 19. Notably, the previously discussed anti-correlation between fine-mode concentration (C_{Vf}) and RRI is evident in the last three inversions: two from October 17 and, to a lesser extent, the final inversion from October 16. This phenomenon, as highlighted earlier, is a common retrieval artifact amplified under conditions such as limited angular radiance measurements caused by cloud cover. The first two inversions from October 16, despite having slightly lower θ_S than the Level 2 threshold of $50°$, appear to provide the most realistic retrievals for both fine-mode concentration and RRI. These retrievals show RRI values ranging between 1.43 and 1.50, consistent with the historical average RRI values for the nine Level 2 inversions from Saint-Denis, and align with expectations for a mixture of biomass burning and sea salt aerosols.

The SSA values for the five R.V. Marion Dufresne inversions range between 0.88 and 0.95, with generally higher absorption observed at longer wavelengths. These values are consistent with the historical average SSA values for the nine Level 2 inversions from Saint-Denis, though they are slightly higher. As in the retrievals from October 12, the varying influence of sea salt aerosols in the mixture could explain the differences with the averaged Saint-Denis values. Additionally, Eck et al. (2013) reported a seasonal trend in SSA during the dry season at three South African sites, with values for pure biomass burning aerosols being highest at the end of the season. Apart from the variation on the sea salt contribution, this trend could also explain the differences with the averaged values, as the period analyzed here is October (while the nine inversions include also retrievals from August, September, and October). While some seasonality may exist, the SSA values retrieved from Saint-

30

Denis on October 19 are notably higher and appear unrealistic for the observed mixture of biomass burning and sea salt aerosols during this week. This discrepancy is likely a result of cloud cover impacting the inversion quality, as retrievals that do not meet Level 2 criteria are expected to exhibit greater uncertainties.

5 Discussion

The overall good performance of the ship-adapted CE318-T photometer onboard the R.V. Marion Dufresne has been demonstrated by the consistent acquisition of high-quality triplets that meet AERONET Level 1.5 criteria, as well as the first successful retrieval of aerosol microphysical and optical properties at sea. These results confirm the system's reliability under conditions typical of large research vessels, which are characterized by limited and slow movements.

To quantify the small and slow movements of the R.V. Marion Dufresne, a full-year analysis was performed using data from 2023, based on consecutive 7-minute segments corresponding to the typical duration of an almucantar scan. For each segment, the mean and standard deviations of pitch and roll were computed to evaluate the amplitude and characteristics of the vessel's motion. An example of such a 7-minute segment is shown in Figure 9, which presents histograms of pitch (left panel) and roll (central panel) measured during an almucantar scan performed at 11:07 UTC on October 16. Dashed lines indicate the mean values, annotated within each panel, while arrows mark the corresponding standard deviations. A fitted normal distribution curve is shown in black, and the data are displayed as shaded histograms with black edges for clarity. It is important to note that the standard deviation provides a direct measure of the amplitude of the vessel's oscillatory motion, while the mean values are more influenced by navigation factors such as heading relative to wave direction or vessel speed. The full-year analysis shows that the standard deviation over 7-minute intervals typically ranges between $0.4°$ and $0.5°$ for both pitch and roll. These statistics include all weather conditions; however, variability tends to be lower during clear-sky periods. For instance, the example shown in Figure 9, recorded under clear-sky and relatively calm conditions, exhibits standard deviations of approximately $0.2°$.

Additionally, the right panel of Figure 9 presents the frequency spectra of these same pitch and roll movements, obtained via a Fast Fourier Transform (FFT), which decomposes the time series into its frequency components. A filtering step was applied to remove the zero-frequency component and focus on oscillatory behavior. The dominant frequencies are found around 0.1Hz (slightly lower for roll and slightly higher for pitch) corresponding to oscillation periods of approximately 10 seconds. These frequency peaks are consistently observed aboard the R.V. Marion Dufresne, indicating that the vessel's oscillations are not only small in amplitude, but also slow in nature.

The success of quality-assured AOD measurements relies on the ability of the continuous tracking system (specifically developed for this marine implementation, as described in subsection 2.1.2) to compensate for oscillations around the vessel's mean orientation. Once the Sun enters the tracking system's field of view (thanks to the initial attitude correction provided by the Trimble ABX-Two), the photometer locks on and maintains alignment through active tracking for the duration of the direct Sun (or Moon) measurement sequence. As shown in Section 3, this implementation performs reliably aboard the R.V. Marion
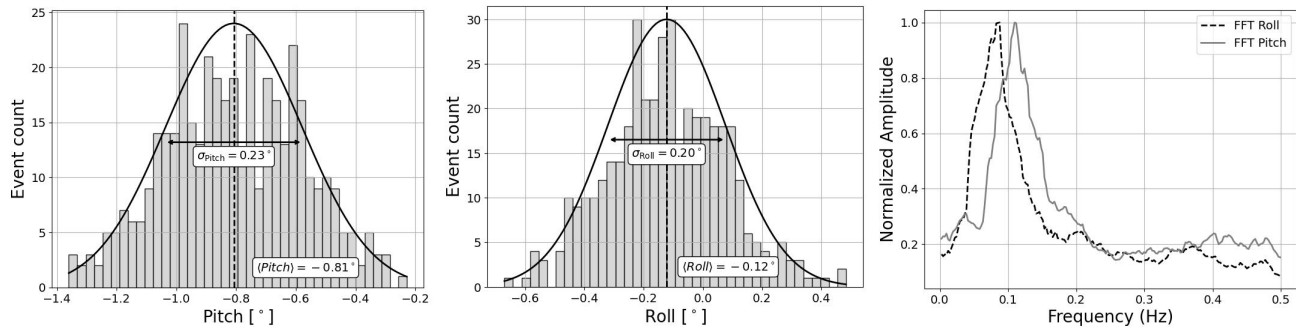
Figure 9. Histograms of pitch (left panel) and roll (central panel) values recorded during the 7-minute almucantar measurement at 11:07 UTC on October 16, 2023. Dashed black lines indicate the mean values, with standard deviations represented by black arrows. A normal distribution curve is also shown. The right panel displays the frequency spectra of pitch and roll motions, derived via FFT.

Dufresne, whose slow and low-amplitude movements fall within the tolerance range of the continuous tracking system. Under these conditions, the instrument consistently yields AOD measurements that meet Level 1.5 quality criteria.

A preliminary analysis of AOD data from similar installations deployed in 2024 on other large research vessels, such as the R.V. Gaia Blu (83 meters, ESA IDEAS-QA4EO program, in collaboration with the Italian Istituto di Scienze Marine del Consiglio Nazionale delle Ricerche) and the R.V. Sarmiento de Balboa (72 meters, in collaboration with Valladolid University and the Consejo Superior de Investigaciones Científicas) confirms that the system is well-adapted for marine aerosol monitoring on large and stable vessels. In these environments, which show motion characteristics similar to those aboard the R.V. Marion Dufresne, AOD Level 1.5 data have also been routinely obtained. Although the data from these new deployments have not yet been analyzed in detail, they hold significant potential for expanding the system's application.

However, despite its robustness on large vessels, the current system faces significant limitations when applied to smaller research vessels. Tests on the 20-meter NOAA R.V. Shearwater, a high-speed catamaran used during the PACE-PAX campaign in September 2024 (https://espo.nasa.gov/pace-pax), showed frequent pitch and roll standard deviations exceeding 2–3°, even under calm conditions. These larger-amplitude motions caused the continuous tracking system to fail, preventing the acquisition of stable Level 1.5 AOD measurements. To address this challenge, a stabilizing mount was tested to actively counteract ship movements while keeping the continuous tracking system operational. This solution successfully enabled Level 1.5 AOD acquisition, achieving similar measurement frequency to that of large vessels. Nevertheless, stabilizing mounts are significantly more expensive (roughly four to five times the cost of the Trimble system) and their long-term resilience in harsh marine environments is still uncertain. In contrast, the Trimble ABX-Two has functioned reliably for three years aboard the R.V. Marion Dufresne without failure. Further testing is needed to evaluate whether stabilizing mounts can offer a sustainable and robust long-term solution for dynamic platforms. An alternative approach currently under development within the Agora Lab involves implementing adaptive, faster tracking based on Proportional-Integral-Derivative (PID) control algorithms. These would adjust tracking speeds dynamically in response to pitch and roll fluctuations, enabling Sun lock even in more turbulent sea conditions.

The shipborne photometer's capabilities extend beyond automatic AOD measurements, as demonstrated by the successful AERONET standard inversions conducted from the R.V. Marion Dufresne (see Section 4), made possible by routine onboard sky radiance acquisitions. The inversions presented in Section 4, although limited to a few days with sufficient aerosol load for quality-assured retrievals (based on AERONET Level 2.0 criteria), show retrieved values consistent with expectations for the region and comparable to historical averages from the nearby Saint-Denis AERONET site. These results confirm the potential for reliable inversions from a moving platform, despite the challenges inherent to shipborne measurements, when conditions are favorable.

Although ship movements are recorded, with the Trimble ABX-Two system generating and storing positioning data every second, the current approach has been to invert radiance measurements using the standard almucantar angles without applying any corrections. The main reason for this choice is that the observed ship movements are generally small as shown in Figure 9. In this regard, a mean pitch and roll value below $1°$ falls within the leveling precision of standard ground-based AERONET stations, as the bubble-level system of the CE318-T introduces a comparable uncertainty in ground-based installations[9]. Additionally, the observed standard deviations are not much higher than the manufacturer's specified error for the Trimble ABX-Two system ($0.1-0.2°$), further questioning both the necessity and the potential accuracy of applying these angular corrections. Moreover, any post-processing correction would disrupt the symmetry criteria used in almucantar and hybrid scans, where left and right branch measurements are traditionally considered symmetric for cloud screening purposes. Given these factors, the most appropriate use of the recorded ship attitude data appears to be as a quality control criterion, requiring mean pitch and roll values to remain below $\pm1°$ and standard deviations below $0.5°$.

These standard deviation values of the ship's movements could be considered comparable to pointing errors in almucantar measurements. The impact of pointing errors on retrieval properties has been analyzed in previous studies. For instance, Dubovik et al. (2000) modeled a $1°$ mispointing in azimuth (twice the threshold suggested here) and found that the only significant effect on inversion products was observed in desert dust retrievals. It is worth noting that the authors did not average the left and right sides of the almucantar (personal communication), so the actual effect would likely be smaller. In a later study, Torres et al. (2014) tested azimuth and zenith errors of $0.4°$ (while also averaging almucantar measurements) and observed minimal influence on almucantar retrievals, even for desert dust. The largest effects were seen in the principal plane scenario, which, unlike almucantar scans, lacks the possibility of averaging and is now obsolete.

The analysis of the heading angle differs slightly from that of pitch and roll. This angle represents the ship's direction and is corrected each time the instrument performs Sun pointing and tracking. For shipborne photometers, this process occurs before each branch of the almucantar measurement (seven wavelengths per branch, left and right), leading to a tracking update approximately every minute. The heading standard deviation observed within one-minute intervals are roughly half the amplitude of pitch and roll variations, suggesting that their impact on almucantar symmetry is even less significant.

---

[9]While the CE318-T is equipped with an internal bubble level, AERONET generally recommends using external leveling systems with higher precision, often achieving level adjustments of 4 mm per meter, corresponding to approximately $0.25°$. However, this recommendation is not always implemented in practice.

Further improvements to mitigate the impact of ship movement on sky radiance measurements could involve actively correcting the photometer's orientation in real-time using pitch and roll information from the attitude system. This approach appears to be a promising long-term and cost-effective solution, as it would eliminate the need for additional mechanical stabilization. However, its implementation would require significant development efforts from the instrument manufacturer, including the integration of dynamic motion compensation algorithms directly into the tracking system. Alternatively, a stabilizing platform, like the one tested on the NOAA R.V. Shearwater, could be used to counteract ship movements and maintain stable pointing. This method would offer the advantage of simplifying post-processing by minimizing the need for attitude corrections. However, it also requires the integration of a costly stabilizing system, which may not be practical for all shipborne deployments.

The primary objective of this study was not to conduct an exhaustive analysis of aerosol inversions but rather to demonstrate the feasibility of performing such measurements and retrieving aerosol optical properties from a moving platform in open ocean conditions. A more detailed validation could not be achieved with the R.V. Marion Dufresne dataset, as only one week with $AOD_{440} > 0.4$ was recorded over a three-year period, and even then, frequent cloud cover further limited the number of quality-assured retrievals, making a more comprehensive analysis unfeasible. Nonetheless, the successful retrievals obtained confirm the potential of shipborne aerosol inversions and establish a foundation for future, more detailed studies. In this regard, the dataset from the R.V. Gaia Blu, which has been operating in the Mediterranean Sea since February 2024, appears to be a strong candidate for a more extensive assessment. A preliminary evaluation of the data recorded by the shipborne photometer onboard R.V. Gaia Blu indicates more frequent episodes with AOD_{440} exceeding 0.4 under clear-sky conditions, including episodes influenced by anthropogenic sources, desert dust, and even volcanic emissions from Etna. Moreover, the frequent proximity of the R.V. Gaia Blu to several Italian ground-based AERONET sites provides an excellent opportunity for a thorough validation of aerosol retrievals by enabling direct comparisons with the same retrievals performed using fixed photometer data. This will allow for an exhaustive assessment of retrieval performance, offering deeper insights into the accuracy and reliability of shipborne aerosol inversions, as well as the influence of ship motion on retrieval quality and potential limitations.

The installations in 2024, along with future deployments foreseen for 2025, will establish a foundation for a new network of ship-based automatic photometers. This network is expected to significantly enhance the study of aerosols in marine environments, particularly in regions that are otherwise challenging to monitor. In addition to supporting systematic aerosol characterization in purely maritime settings, this network will contribute to the validation of satellite observations. It will provide valuable ground-truth data not only for AOD product but also for more complex aerosol optical properties, such SSA. These data will be critical for validating the advanced retrievals from upcoming multi-angular polarimetric sensors onboard space missions, such as the ESA-EUMETSAT 3MI/MetOp-SG and NASA's PACE mission, which includes the SpexOne and HARP2 sensors (details and other mission sensors in Dubovik et al., 2019).

6   Conclusions

This study demonstrates the feasibility of establishing a permanent AERONET site aboard research vessels, adhering to the same automated measurement protocols and standards as conventional ground-based sites. Over a three-year period (July

2021–June 2024), the first ship-based AERONET site equipped with automatic photometer measurements was operated aboard the R.V. Marion Dufresne, primarily in the southwestern Indian Ocean, collecting a continuous AOD dataset as part of MAP-IO program. The mean AOD values—0.093 ± 0.075, 0.063 ± 0.041, and 0.054 ± 0.031 at 440, 675, and 870 nm, respectively—are consistent with previous studies characterizing aerosols in uncontaminated marine environments. Similarly, the average α of 0.76 ± 0.40 reflects the dominance of coarse-mode aerosols, with episodic contributions from fine-mode aerosols.

The reliability and precision of the ship-adapted CE318-T photometer were validated through detailed intercomparisons, particularly during the Amaryllis-Amagas/Transama campaign. During this campaign, two photometers (#1273 and #1243) were simultaneously operated aboard the R.V. Marion Dufresne between April and June 2023, enabling a direct comparison of their measurements. Strong correlations (R > 0.965) were observed across all analyzed AOD wavelengths (380–870 nm), with RMSE values ranging from 0.005 to 0.008, and biases between -8.2×10^{-5} and 4.2×10^{-3}. These results confirm the high precision of the shipborne system and are comparable to those reported by Yin et al. (2019), who analyzed CE318-T measurements against MAN Microtops-II observations during the OCEANET campaigns aboard the R.V. Polarstern, finding RMSE values of 0.009–0.015 (their Figure 4). Notably, the strong correlations and minimal biases observed in AOD comparisons during this study align with those typically obtained at ground-based calibration sites during intercalibration periods with AERONET master instruments. This consistency underscores the reliability of shipborne Level 1.5 data, reinforcing its comparability to well-established AERONET standards.

In addition to co-located comparisons, the shipborne photometer was validated against the AERONET ground-based site at Saint-Denis, located 93 meters above sea level and approximately 20 km from the port of La Réunion. A systematic negative bias was observed in the shipborne AOD data relative to Saint-Denis, ranging from -7.0×10^{-3} to -1.3×10^{-2}, which can be attributed to altitude differences and variations in local aerosol sources. While Saint-Denis is considered a relatively clean urban site, the R.V. Marion Dufresne is frequently docked in Le Port, an area influenced by industrial emissions, including those from a coal-fired power plant. Similarly, α exhibited a positive bias of 0.08, likely reflecting a greater contribution of fine-mode aerosols at Saint-Denis, where the reduced influence of marine aerosols allows urban aerosol contributions to become more dominant (Duflot et al., 2022). Despite these systematic differences, the strong correlations observed between the shipborne and ground-based measurements (R = 0.86–0.93) demonstrate that both instruments capture similar temporal aerosol variability, further supporting the reliability of shipborne photometer.

A key achievement of this study is the successful application of the AERONET aerosol inversion algorithm to shipborne platforms, resulting in the first quality-assured retrievals of aerosol microphysical and optical properties from a moving research vessel. The data obtained during the exceptional biomass burning event of October 2023 exemplify the system's capability to perform advanced aerosol characterization in remote marine environments. During this episode, AOD_{440} values frequently exceeded 0.36, peaking at 0.73, and α values averaged 1.56, highlighting a clear shift from background marine conditions to a fine-mode-dominated regime. Backward trajectory analyses confirmed the predominant influence of fine-mode aerosols transported from Madagascar, where intense biomass burning activity was occurring.

Retrievals of aerosol microphysical and optical properties during this period from measurements aboard the R.V. Marion Dufresne were presented alongside those from the Saint-Denis site in Figures 7 (for the coincident day, October 12, at both

sites) and 8 (for non-coincident days between the two sites). The retrieved fine-mode modal radii (R_{Vf}), summarized in Table 3,
remained remarkably consistent across inversions from both the shipborne platform and the Saint-Denis site, ranging from 0.13
to 0.18 μm. This consistency underscores the ability of the shipborne photometer to accurately characterize fine-mode particle
size during biomass burning episodes. However, fine-mode volume concentrations (C_{Vf}) derived from the shipborne photome-
ter were consistently higher than those retrieved at Saint-Denis. This discrepancy can be attributed to the well-documented
anti-correlation between fine-mode volume concentration and refractive index (Herrera et al., 2022), which may be further
amplified in inversions where limited angular radiance data, due to cloud cover, influences retrieval accuracy.

As noted by Sinyuk et al. (2020), even in cases with marked anti-correlation between fine-mode volume concentration and
refractive index, the AERONET retrieval algorithm reliably distinguishes between aerosol absorption and scattering properties.
Indeed, the SSA retrievals from the shipborne platform exhibit robust performance, with values ranging from 0.88 to 0.95,
indicating increased absorption at longer wavelengths. These SSA values are consistent with expectations for a mixture of
biomass burning and sea salt aerosols (Dubovik et al., 2002b). Moreover, the SSA values obtained during this week closely
match with historical data from the Saint-Denis site under high aerosol load conditions, meeting the $AOD_{440} > 0.4$ threshold
required for AERONET Level 2 criteria.

In conclusion, the deployment of a CE318-T photometer aboard the R.V. Marion Dufresne has demonstrated its viability
for providing high-quality aerosol measurements comparable to those of AERONET ground-based stations. These findings
validate the system's potential to close observational gaps in marine aerosol research, offering a novel approach for satellite
validation and advancing our understanding of aerosol-climate interactions in remote oceanic environments.

Acronyms and Symbols

Table 4. List of acronyms and symbols used in the manuscript.

Acronym / Symbol	Meaning
AERONET	Aerosol Robotic Network
AOD	Aerosol Optical Depth
AOD_x	Aerosol Optical Depth at wavelength x nm
CE318-T	Cimel Electronique Sun Sky Lunar Multispectral Photometer model CE318-T
C_{Vf}	Fine-mode volume concentration (column-integrated volume size distribution) $[\mu m^3/\mu m^2]$
C_{Vc}	Coarse-mode volume concentration (column-integrated volume size distribution) $[\mu m^3/\mu m^2]$
DN	Digital Number
GPS	Global Positioning System
Ifremer	Institut Français de Recherche pour l'Exploitation de la Mer
IPCC	Intergovernmental Panel on Climate Change
L1.0, L1.5, L2.0	AERONET data levels (preliminary processed, cloud-screened, quality-assured)
MAN	Maritime Aerosol Network
MAP-IO	Marion Dufresne Atmospheric Program – Indian Ocean
MODIS	Moderate Resolution Imaging Spectroradiometer
NASA	National Aeronautics and Space Administration
NOAA	National Oceanic and Atmospheric Administration
PWV	Precipitable Water Vapor
R	Pearson correlation coefficient
R_{eff}	Total column effective radius of volume size distribution $[\mu m]$
R_{Vf}	Fine-mode modal radius of volume size distribution $[\mu m]$
R_{Vc}	Coarse-mode modal radius of volume size distribution $[\mu m]$
RMSE	Root-Mean-Square Error
RRI	Real part of refractive index
RRI_x	Real part of refractive index at wavelength x nm
R.V.	Research Vessel
SSA	Single Scattering Albedo
SSA_x	Single Scattering Albedo at wavelength x nm
TAAF	Terres Australes et Antarctiques Françaises
α	Ångström exponent (computed over the 440–870 nm range)
λ	Wavelength
θ_S	Solar Zenith Angle

References

Albrecht, B. A.: Aerosols, Cloud Microphysics, and Fractional Cloudiness, Science, 245, 1227–1230, https://doi.org/10.1126/science.245.4923.1227, 1989.

Alterskjær, K. and Kristjánsson, J. E.: The sign of the radiative forcing from marine cloud brightening depends on both particle size and injection amount, Geophys. Res. Lett., 40, 210–215, https://doi.org/10.1029/2012GL054286, 2013.

Ångström, A.: On the Atmospheric Transmission of Sun Radiation and on Dust in the Air, Geogr. Ann., 11, 156–166, https://doi.org/10.2307/519399, 1929.

Barreto, A., Cuevas, E., Damiri, B., Guirado, C., Berkoff, T., Berjón, A. J., Hernández, Y., Almansa, F., and Gil, M.: A new method for nocturnal aerosol measurements with a lunar photometer prototype, Atmos. Meas. Tech., 6, 585–598, https://doi.org/10.5194/amt-6-585-2013, 2013.

Barreto, A., Cuevas, E., Granados-Muñoz, M., Alados-Arboledas, L., Romero, P. M., Gröbner, J., Kouremeti, N., Almansa, A. F., Stone, T., Toledano, C., Román, R., Sorokin, M., Holben, B., Canini, M., and Yela, M.: The new sun-sky-lunar Cimel CE318-T multiband photometer – a comprehensive performance evaluation, Atmos. Meas. Tech., 9, 631–654, https://doi.org/10.5194/amt-9-631-2016, 2016.

Blanchard, D. C. and Woodcock, A. H.: The production, concentration, and vertical distribution of the sea-salt aerosol, Ann. N. Y. Acad. Sci., 338, 330–347, https://doi.org/10.1111/j.1749-6632.1980.tb17130.x, 1980.

Chen, C., Dubovik, O., Fuertes, D., Litvinov, P., Lapyonok, T., Lopatin, A., Ducos, F., Derimian, Y., Herman, M., Tanré, D., Remer, L. A., Lyapustin, A., Sayer, A. M., Levy, R. C., Hsu, N. C., Descloitres, J., Li, L., Torres, B., Karol, Y., Herrera, M., Herreras, M., Aspetsberger, M., Wanzenboeck, M., Bindreiter, L., Marth, D., Hangler, A., and Federspiel, C.: Validation of GRASP algorithm product from POLDER/PARASOL data and assessment of multi-angular polarimetry potential for aerosol monitoring, Earth Syst. Sci. Data, 12, 3573–3620, https://doi.org/10.5194/essd-12-3573-2020, 2020.

Clain, G., Baray, J. L., Delmas, R., Diab, R., Leclair de Bellevue, J., Keckhut, P., Posny, F., Metzger, J. M., and Cammas, J. P.: Tropospheric ozone climatology at two Southern Hemisphere tropical/subtropical sites, (Reunion Island and Irene, South Africa) from ozonesondes, LIDAR, and in situ aircraft measurements, Atmos. Chem. Phys., 9, 1723–1734, https://doi.org/10.5194/acp-9-1723-2009, 2009.

de Leeuw, G., Andreas, E. L., Anguelova, M. D., Fairall, C. W., Lewis, E. R., O'Dowd, C., Schulz, M., and Schwartz, S. E.: Production flux of sea spray aerosol, Rev. Geophys., 49, https://doi.org/10.1029/2010RG000349, 2011.

Denjean, C., Bourrianne, T., Burnet, F., Mallet, M., Maury, N., Colomb, A., Dominutti, P., Brito, J., Dupuy, R., Sellegri, K., Schwarzenboeck, A., Flamant, C., and Knippertz, P.: Overview of aerosol optical properties over southern West Africa from DACCIWA aircraft measurements, Atmos. Chem. Phys., 20, 4735–4756, https://doi.org/10.5194/acp-20-4735-2020, 2020.

Dubovik, O. and King, M. D.: A flexible inversion algorithm for retrieval of aerosol optical properties from Sun and sky radiance measurements, J. Geophys. Res. Atmos., 105, 20 673–20 696, https://doi.org/10.1029/2000JD900282, 2000.

Dubovik, O., Smirnov, A., Holben, B. N., King, M. D., Kaufman, Y. J., Eck, T. F., and Slutsker, I.: Accuracy assessments of aerosol optical properties retrieved from Aerosol Robotic Network (AERONET) Sun and sky radiance measurements, J. Geophys. Res. Atmos., 105, 9791–9806, https://doi.org/10.1029/2000JD900040, 2000.

Dubovik, O., Holben, B., Eck, T. F., Smirnov, A., Kaufman, Y. J., King, M., Tanré, D., and Slutsker, I.: Variability of absorption and optical properties of key aerosol types observed in worldwide locations, J. Atmos. Sci., 59, 590–608, https://doi.org/10.1175/1520-0469(2002)059<0590:VOAAOP>2.0.CO;2, 2002a.

990 Dubovik, O., Holben, B. N., Lapyonok, T., Sinyuk, A., Mishchenko, M., Yang, P., and Slutsker, I.: Non-spherical aerosol retrieval method employing light scattering by spheroids, Geophys. Res. Lett., 29, 54/1–4, https://doi.org/10.1029/2001GL014506, 2002b.

Dubovik, O., Sinyuk, A., Lapyonok, T., Holben, B. N., Mishchenko, M., Yang, P., Eck, T. F., Volten, H., Munoz, O., Veihelmann, B., Van Der Zande, W. J., Leon, J. F., Sorokin, M., and Slutsker, I.: Application of spheroid models to account for aerosol particle nonsphericity in remote sensing of desert dust, J. Geophys. Res. Atmos., 111, D11 208, https://doi.org/10.1029/2005JD006619, 2006.

995 Dubovik, O., Herman, M., Holdak, A., Lapyonok, T., Tanré, D., Deuzé, J. L., Ducos, F., Sinyuk, A., and Lopatin, A.: Statistically optimized inversion algorithm for enhanced retrieval of aerosol properties from spectral multi-angle polarimetric satellite observations, Atmos. Meas. Tech., 4, 975–1018, https://doi.org/10.5194/amt-4-975-2011, 2011.

Dubovik, O., Li, Z., Mishchenko, M. I., Tanré, D., Karol, Y., Bojkov, B., Cairns, B., Diner, D. J., Espinosa, W. R., Goloub, P., Gu, X., Hasekamp, O., Hong, J., Hou, W., Knobelspiesse, K. D., Landgraf, J., Li, L., Litvinov, P., Liu, Y., Lopatin, A., Marbach, T., Maring, H.,
1000 Martins, V., Meijer, Y., Milinevsky, G., Mukai, S., Parol, F., Qiao, Y., Remer, L., Rietjens, J., Sano, I., Stammes, P., Stamnes, S., Sun, X., Tabary, P., Travis, L. D., Waquet, F., Xu, F., Yan, C., and Yin, D.: Polarimetric remote sensing of atmospheric aerosols: Instruments, methodologies, results, and perspectives, J. Quant. Spectrosc. Radiat. Transf., 224, 474–511, https://doi.org/10.1016/j.jqsrt.2018.11.024, 2019.

Duflot, V., Dils, B., Baray, J. L., De Mazière, M., Attié, J. L., Vanhaelewyn, G., Senten, C., Vigouroux, C., Clain, G., and Delmas, R.:
1005 Analysis of the origin of the distribution of CO in the subtropical southern Indian Ocean in 2007, J. Geophys. Res.-Atmos., 115, https://doi.org/10.1029/2010JD013994, 2010.

Duflot, V., Bègue, N., Pouliquen, M.-L., Goloub, P., and Metzger, J.-M.: Aerosols on the Tropical Island of La Réunion (21°S, 55°E): Assessment of Climatology, Origin of Variability and Trend, Remote Sensing, 14, https://doi.org/10.3390/rs14194945, 2022.

Eck, T. F., Holben, B. N., Reid, J. S., Dubovik, O., Smirnov, A., O'Neill, N., Slutsker, I., and Kinne, S.: Wavelength depen-
1010 dence of the optical depth of biomass burning, urban, and desert dust aerosols, J. Geophys. Res. Atmos., 104, 31 333–31 349, https://doi.org/10.1029/1999JD900923, 1999.

Eck, T. F., Holben, B. N., Reid, J. S., Mukelabai, M. M., Piketh, S. J., Torres, O., Jethva, H. T., Hyer, E. J., Ward, D. E., Dubovik, O., Sinyuk, A., Schafer, J. S., Giles, D. M., Sorokin, M., Smirnov, A., and Slutsker, I.: A seasonal trend of single scattering albedo in southern African biomass-burning particles: Implications for satellite products and estimates of emissions for the world's largest biomass-burning source,
1015 J. Geophys. Res.-Atmos., 118, 6414–6432, https://doi.org/10.1002/jgrd.50500, 2013.

Eck, T. F., Holben, B. N., Reid, J. S., Xian, P., Giles, D. M., Sinyuk, A., Smirnov, A., Schafer, J. S., Slutsker, I., Kim, J., Koo, J.-H., Choi, M., Kim, K. C., Sano, I., Arola, A., Sayer, A. M., Levy, R. C., Munchak, L. A., O'Neill, N. T., Lyapustin, A., Hsu, N. C., Randles, C. A., Da Silva, A. M., Buchard, V., Govindaraju, R. C., Hyer, E., Crawford, J. H., Wang, P., and Xia, X.: Observations of the Interaction and Transport of Fine Mode Aerosols With Cloud and/or Fog in Northeast Asia From Aerosol Robotic Network and Satellite Remote Sensing,
1020 J. Geophys. Res.-Atmos., 123, 5560–5587, https://doi.org/10.1029/2018JD028313, 2018.

Eger, P. G., Friedrich, N., Schuladen, J., Shenolikar, J., Fischer, H., Tadic, I., Harder, H., Martinez, M., Rohloff, R., Tauer, S., Drewnick, F., Fachinger, F., Brooks, J., Darbyshire, E., Sciare, J., Pikridas, M., Lelieveld, J., and Crowley, J. N.: Shipborne measurements of ClNO$_2$ in the Mediterranean Sea and around the Arabian Peninsula during summer, Atmos. Chem. Phys., 19, 12 121–12 140, https://doi.org/10.5194/acp-19-12121-2019, 2019.

1025 Facchini, M. C., Rinaldi, M., Decesari, S., Carbone, C., Finessi, E., Mircea, M., Fuzzi, S., Ceburnis, D., Flanagan, R., Nilsson, E. D., de Leeuw, G., Martino, M., Woeltjen, J., and O'Dowd, C. D.: Primary submicron marine aerosol dominated by insoluble organic colloids and aggregates, Geophys. Res. Lett., 35, https://doi.org/10.1029/2008GL034210, 2008.

Fargion, G. S., McClain, C. R., and Barnes, R. A.: Ocean color instrument intercomparisons and cross-calibrations by the SIMBIOS project (1999-2000), in: Proc. SPIE 4135, pp. 411 – 420, Earth Observing Systems V, https://doi.org/10.1117/12.494210, 2000.

1030 Fargion, G. S., Franz, B. A., Kwiatkowska, E. J., Pietras, C. M., Bailey, S. W., Gales, J., Meister, G., Knobelspiesse, K. D., Werdell, J., and McClain, C. R.: SIMBIOS program in support of ocean color missions: 1997-2003, in: Proc. SPIE 5155, pp. 49 – 60, Ocean Remote Sensing and Imaging II, https://doi.org/10.1117/12.504769, 2003.

Fedarenka, A., Dubovik, O., Goloub, P., Li, Z., Lapyonok, T., Litvinov, P., Barel, L., Gonzalez, L., Podvin, T., and Crozel, D.: Utilization of AERONET polarimetric measurements for improving retrieval of aerosol microphysics: GSFC, Beijing and Dakar data analysis, J. Quant.

1035 Spectrosc. Radiat. Transf., 179, 72–97, https://doi.org/10.1016/j.jqsrt.2016.03.021, 2016.

Fitzgerald, J. W.: Marine aerosols: A review, Atmos. Environ. Part A. General Topics, 25, 533–545, https://doi.org/10.1016/0960-1686(91)90050-H, 1991.

Gantt, B. and Meskhidze, N.: The physical and chemical characteristics of marine primary organic aerosol: a review, Atmos. Chem. Phys., 13, 3979–3996, https://doi.org/10.5194/acp-13-3979-2013, 2013.

1040 Gantt, B., Meskhidze, N., Facchini, M. C., Rinaldi, M., Ceburnis, D., and O'Dowd, C. D.: Wind speed dependent size-resolved parameterization for the organic mass fraction of sea spray aerosol, Atmos. Chem. Phys., 11, 8777–8790, https://doi.org/10.5194/acp-11-8777-2011, 2011.

Gathman, S. G.: Optical Properties Of The Marine Aerosol As Predicted By The Navy Aerosol Model, Opt. Eng., 22, 220 157, https://doi.org/10.1117/12.7973048, 1983.

1045 Giglio, L., Descloitres, J., Justice, C. O., and Kaufman, Y. J.: An Enhanced Contextual Fire Detection Algorithm for MODIS, Remote Sens. Environ., 87, 273–282, https://doi.org/10.1016/S0034-4257(03)00184-6, 2003.

Giles, D. M., Holben, B. N., Eck, T. F., Sinyuk, A., Smirnov, A., Slutsker, I., Dickerson, R. R., Thompson, A. M., and Schafer, J. S.: An analysis of AERONET aerosol absorption properties and classifications representative of aerosol source regions, J. Geophys. Res.-Atmos., 117, https://doi.org/10.1029/2012JD018127, 2012.

1050 Giles, D. M., Sinyuk, A., Sorokin, M. G., Schafer, J. S., Smirnov, A., Slutsker, I., Eck, T. F., Holben, B. N., Lewis, J. R., Campbell, J. R., Welton, E. J., Korkin, S. V., and Lyapustin, A. I.: Advancements in the Aerosol Robotic Network (AERONET) Version 3 database – automated near-real-time quality control algorithm with improved cloud screening for Sun photometer aerosol optical depth (AOD) measurements, Atmos. Meas. Tech., 12, 169–209, https://doi.org/10.5194/amt-12-169-2019, 2019.

Gordon, H. R. and Clark, D. K.: Clear water radiances for atmospheric correction of coastal zone color scanner imagery, Appl. Opt., 20, 1055 4175–4180, https://doi.org/10.1364/AO.20.004175, 1981.

Gunn, R. and Phillips, B. B.: An experimental investigation of the effect of air pollution on the initiation of rain, J. Atmos. Sci., 14, 272 – 280, https://doi.org/10.1175/1520-0469(1957)014<0272:AEIOTE>2.0.CO;2, 1957.

Gupta, P., Levy, R. C., Mattoo, S., Remer, L. A., and Munchak, L. A.: A surface reflectance scheme for retrieving aerosol optical depth over urban surfaces in MODIS Dark Target retrieval algorithm, Atmos. Meas. Tech., 9, 3293–3308, https://doi.org/10.5194/amt-9-3293-2016, 1060 2016.

Gupta, P., Remer, L. A., Levy, R. C., and Mattoo, S.: Validation of MODIS 3 km land aerosol optical depth from NASA's EOS Terra and Aqua missions, Atmos. Meas. Tech., 11, 3145–3159, https://doi.org/10.5194/amt-11-3145-2018, 2018.

Hamilton, D. S., Lee, L. A., Pringle, K. J., Reddington, C. L., Spracklen, D. V., and Carslaw, K. S.: Occurrence of pristine aerosol environments on a polluted planet, Proc. Natl. Acad. Sci., 111, 18 466–18 471, https://doi.org/10.1073/pnas.1415440111, 2014.

1065 Haywood, J. M., Ramaswamy, V., and Soden, B. J.: Tropospheric Aerosol Climate Forcing in Clear-Sky Satellite Observations over the Oceans, Science, 283, 1299–1303, https://doi.org/10.1126/science.283.5406.1299, 1999.

Herrera, M. E., Dubovik, O., Torres, B., Lapyonok, T., Fuertes, D., Lopatin, A., Litvinov, P., Chen, C., Benavent-Oltra, J. A., Bali, J. L., and Ristori, P. R.: Estimates of remote sensing retrieval errors by the GRASP algorithm: application to ground-based observations, concept and validation, Atmos. Meas. Tech., 15, 6075–6126, https://doi.org/10.5194/amt-15-6075-2022, 2022.

1070 Holben, B. N., Eck, T. F., Slutsker, I., Tanré, D., Buis, J. P., Setzer, A., Vermote, E., Reagan, J. A., Kaufman, Y. J., Nakajima, T., Lavenu, F., Jankowiak, I., and Smirnov, A.: AERONET - A federated instrument network and data archive for aerosol characterization, Remote Sens. Environ., 66, 1–16, https://doi.org/10.1016/S0034-4257(98)00031-5, 1998.

Holben, B. N., Tanré, D., Smirnov, A., Eck, T. F., Slutsker, I., Abuhassan, N., Newcomb, W. W., Schafer, J. S., Chatenet, B., Lavenu, F., Kaufman, Y. J., Castle, J. V., Setzer, A., Markham, B., Clark, D., Frouin, R., Halthore, R., Karneli, A., O'Neill, N. T., Pietras, C., Pinker, 1075 R. T., Voss, K., and Zibordi, G.: An emerging ground-based aerosol climatology: Aerosol optical depth from AERONET, J. Geophys. Res.-Atmos., 106, 12 067–12 097, https://doi.org/10.1029/2001JD900014, 2001.

Holben, B. N., Eck, T. F., Slutsker, I., Smirnov, A., Sinyuk, A., Schafer, J., Giles, D., and Dubovik, O.: AERONET's Version 2.0 quality assurance criteria, in: Proc. SPIE 6408, Remote Sensing of the Atmosphere and Clouds, 6408Q, https://doi.org/10.1117/12.706524, 2006.

Hoppel, W. A., Fitzgerald, J. W., Frick, G. M., Larson, R. E., and Mack, E. J.: Aerosol size distributions and optical properties found in 1080 the marine boundary layer over the Atlantic Ocean, J. Geophys. Res.-Atmos., 95, 3659–3686, https://doi.org/10.1029/JD095iD04p03659, 1990.

Intergovernmental Panel on Climate Change (IPCC): Climate Change 2021 – The Physical Science Basis: Working Group I Contribution to the Sixth Assessment Report of the Intergovernmental Panel on Climate Change, Cambridge University Press, Cambridge, UK, https://doi.org/doi:10.1017/9781009157896, 2021.

1085 Jones, A., Haywood, J. M., and Boucher, O.: Aerosol forcing, climate response and climate sensitivity in the Hadley Centre climate model, J. Geophys. Res.-Atmos., 112, https://doi.org/10.1029/2007JD008688, 2007.

Karol, Y., Tanré, D., Goloub, P., Vervaerde, C., Balois, J. Y., Blarel, L., Podvin, T., Mortier, A., and Chaikovsky, A.: Airborne sun photometer PLASMA: concept, measurements, comparison of aerosol extinction vertical profile with lidar, Atmos. Meas. Tech., 6, 2383–2389, https://doi.org/10.5194/amt-6-2383-2013, 2013.

1090 Kaskaoutis, D., Pikridas, M., Barmpounis, K., Kassell, G., Logan, D., Rigler, M., Ivančič, M., Mohammadpour, K., Mihalopoulos, N., Lelieveld, J., and Sciare, J.: Aerosol characteristics and types in the marine environments surrounding the East Mediterranean - Middle East (EMME) region during the AQABA campaign, Atmos. Environ., 298, 119 633, https://doi.org/10.1016/j.atmosenv.2023.119633, 2023.

Knobelspiesse, K. D., Pietras, C., Fargion, G. S., Wang, M., Frouin, R., Miller, M. A., Subramaniam, A., and Balch, W. M.: Maritime aerosol 1095 optical thickness measured by handheld sun photometers, Remote Sens. Environ., 93, 87–106, https://doi.org/10.1016/j.rse.2004.06.018, 2004.

Kobayashi, H. and Shiobara, M.: Development of new shipborne aureolemeter to measure the intensities of direct and scattered solar radiation on rolling and pitching vessel, in: Remote Sensing of Clouds and the Atmosphere XX, edited by Comerón, A., Kassianov, E. I., and Schäfer, K., vol. 9640, p. 96401A, International Society for Optics and Photonics, SPIE, https://doi.org/10.1117/12.2195691, 2015.

1100 Koren, I., Dagan, G., and Altaratz, O.: From aerosol-limited to invigoration of warm convective clouds, Science, 344, 1143–1146, https://doi.org/10.1126/science.1252595, 2014.

Leck, C. and Bigg, E. K.: Comparison of sources and nature of the tropical aerosol with the summer high Arctic aerosol, Tellus B: Chemical and Physical Meteorology, 60, 118–126, https://doi.org/10.1111/j.1600-0889.2007.00315.x, 2008.

Levy, R. C., Mattoo, S., Munchak, L. A., Remer, L. A., Sayer, A. M., Patadia, F., and Hsu, N. C.: The Collection 6 MODIS aerosol products over land and ocean, Atmos. Meas. Tech., 6, 2989–3034, https://doi.org/10.5194/amt-6-2989-2013, 2013.

Lewis, E. R. and Schwartz, S. E.: Sea Salt Aerosol Production: Mechanisms, Methods, Measurements and Models—A Critical Review, Geophys. Monogr. Ser., 152, 3719, https://doi.org/10.1029/GM152, 2004.

Mahowald, N. M., Lamarque, J.-F., Tie, X. X., and Wolff, E.: Sea-salt aerosol response to climate change: Last Glacial Maximum, preindustrial, and doubled carbon dioxide climates, J. Geophys. Res.-Atmos., 111, https://doi.org/10.1029/2005JD006459, 2006.

Mallet, M., Nabat, P., Zuidema, P., Redemann, J., Sayer, A. M., Stengel, M., Schmidt, S., Cochrane, S., Burton, S., Ferrare, R., Meyer, K., Saide, P., Jethva, H., Torres, O., Wood, R., Saint Martin, D., Roehrig, R., Hsu, C., and Formenti, P.: Simulation of the transport, vertical distribution, optical properties and radiative impact of smoke aerosols with the ALADIN regional climate model during the ORACLES-2016 and LASIC experiments, Atmos. Chem. Phys., 19, 4963–4990, https://doi.org/10.5194/acp-19-4963-2019, 2019.

Mallet, P., Pujol, O., Brioude, J., Evan, S., and A., J.: Marine aerosol distribution and variability over the pristine Southern Indian Ocean, Atmos. Environ., 182, 17–30, https://doi.org/10.1016/j.atmosenv.2018.03.016, 2018.

O'Dowd, C. D. and de Leeuw, G.: Marine aerosol production: a review of the current knowledge, Philos. Trans. R. Soc. A, 365, 1753–1774, https://doi.org/10.1098/rsta.2007.2043, 2007.

O'Dowd, C. D. and Smith, M. H.: Physicochemical properties of aerosols over the northeast Atlantic: Evidence for wind-speed-related submicron sea-salt aerosol production, J. Geophys. Res.-Atmos., 98, 1137–1149, https://doi.org/10.1029/92JD02302, 1993.

O'Dowd, C. D., Smith, M. H., Consterdine, I. E., and Lowe, J. A.: Marine aerosol, sea-salt, and the marine sulphur cycle: a short review, Atmos. Environ., 31, 73–80, https://doi.org/10.1016/S1352-2310(96)00106-9, 1997.

O'Dowd, C. D., Lowe, J. A., and Smith, M. H.: Coupling sea-salt and sulphate interactions and its impact on cloud droplet concentration predictions, Geophys. Res. Lett., 26, 1311–1314, https://doi.org/10.1029/1999GL900231, 1999.

O'Dowd, C. D., Yoon, Y. J., Junkerman, W., Aalto, P., Kulmala, M., Lihavainen, H., and Viisanen, Y.: Airborne measurements of nucleation mode particles I: coastal nucleation and growth rates, Atmos. Chem. Phys., 7, 1491–1501, https://doi.org/10.5194/acp-7-1491-2007, 2007.

Pfannerstill, E. Y., Wang, N., Edtbauer, A., Bourtsoukidis, E., Crowley, J. N., Dienhart, D., Eger, P. G., Ernle, L., Fischer, H., Hottmann, B., Paris, J.-D., Stönner, C., Tadic, I., Walter, D., Lelieveld, J., and Williams, J.: Shipborne measurements of total OH reactivity around the Arabian Peninsula and its role in ozone chemistry, Atmos. Chem. Phys., 19, 11 501–11 523, https://doi.org/10.5194/acp-19-11501-2019, 2019.

Porter, J. N. and Clarke, A. D.: Aerosol size distribution models based on in situ measurements, J. Geophys. Res.-Atmos., 102, 6035–6045, https://doi.org/10.1029/96JD03403, 1997.

Pringle, K. J., Carslaw, K. S., Fan, T., Mann, G. W., Hill, A., Stier, P., Zhang, K., and Tost, H.: A multi-model assessment of the impact of sea spray geoengineering on cloud droplet number, Atmos. Chem. Phys., 12, 11 647–11 663, https://doi.org/10.5194/acp-12-11647-2012, 2012.

Prospero, J. M., Ginoux, P., Torres, O., Nicholson, S. E., and Gill, T. E.: Environmental characterization of global sources of atmospheric soil dust identified with the Nimbus 7 Total Ozone Mapping Spectrometer (TOMS) absorbing aerosol product, Rev. Geophys., 40, 2–1–2–31, https://doi.org/10.1029/2000RG000095, 2002.

Russell, L. M., Hawkins, L. N., Frossard, A. A., Quinn, P. K., and Bates, T. S.: Carbohydrate-like composition of submicron atmospheric particles and their production from ocean bubble bursting, Proc. Natl. Acad. Sci., 107, 6652–6657, https://doi.org/10.1073/pnas.0908905107, 2010.

Sanchez-Barrero, M. F.: Development of an autonomous integrated mobile system combining lidar and photometer to monitor aerosol properties in near real time., Ph.D. thesis, Université de Lille, https://pepite.univ-lille.fr/ori-oai-search/notice/view/2024ULILR014, 2024.

Sandu, I., Brenguier, J.-L., Geoffroy, O., Thouron, O., and Masson, V.: Aerosol Impacts on the Diurnal Cycle of Marine Stratocumulus, J. Atmos. Sci., 65, 2705 – 2718, https://doi.org/10.1175/2008JAS2451.1, 2008.

Satheesh, S. and Krishna Moorthy, K.: Radiative effects of natural aerosols: A review, Atmos. Environ., 39, 2089–2110, https://doi.org/10.1016/j.atmosenv.2004.12.029, 2005.

Sayer, A., Hsu, N., Lee, J., Kim, W. V., Dubovik, O., Dutcher, S., Huang, D., Litvinov, P., Lyapustin, A., Tackett, J., and Winker, D.: Validation of SOAR VIIRS Over-Water Aerosol Retrievals and Context Within the Global Satellite Aerosol Data Record, J. Geophys. Res.-Atmos., 123, 13,496–13,526, https://doi.org/10.1029/2018JD029465, 2018.

Schuster, G. L., Lin, B., and Dubovik, O.: Remote sensing of aerosol water uptake, Geophys. Res. Lett., 36, https://doi.org/10.1029/2008GL036576, 2009.

Shaw, G. E.: Sun Photometry., Bull. Am. Meteorol. Soc., 64, 4–10, https://doi.org/10.1175/1520-0477(1983)064<0004:SP>2.0.CO;2, 1983.

Sinyuk, A., Holben, B. N., Eck, T. F., Giles, D. M., Slutsker, I., Korkin, S., Schafer, J. S., Smirnov, A., Sorokin, M., and Lyapustin, A.: The AERONET Version 3 aerosol retrieval algorithm, associated uncertainties and comparisons to Version 2, Atmos. Meas. Tech., 13, 3375–3411, https://doi.org/10.5194/amt-13-3375-2020, 2020.

Smirnov, A., Holben, B. N., Kaufman, Y. J., Dubovik, O., Eck, T. F., Slutsker, I., Pietras, C., and Halthore, R.: Optical properties of atmospheric aerosol in maritime environments, J. Atmos. Sci., 59, 501–523, https://doi.org/10.1175/1520-0469(2002)059<0501:OPOAAI>2.0.CO;2, 2002.

Smirnov, A., Holben, B. N., Slutsker, I., Giles, D. M., McClain, C. R., Eck, T. F., Sakerin, S. M., Macke, A., Croot, P., Zibordi, G., Quinn, P. K., Sciare, J., Kinne, S., Harvey, M., Smyth, T. J., Piketh, S., Zielinski, T., Proshutinsky, A., Goes, J. I., Nelson, N. B., Larouche, P., Radionov, V. F., Goloub, P., Krishna Moorthy, K., Matarrese, R., Robertson, E. J., and Jourdin, F.: Maritime Aerosol Network as a component of Aerosol Robotic Network, J. Geophys. Res.-Atmos., 114, https://doi.org/10.1029/2008JD011257, 2009.

Smirnov, A., Holben, B. N., Giles, D. M., Slutsker, I., O'Neill, N. T., Eck, T. F., Macke, A., Croot, P., Courcoux, Y., Sakerin, S. M., Smyth, T. J., Zielinski, T., Zibordi, G., Goes, J. I., Harvey, M. J., Quinn, P. K., Nelson, N. B., Radionov, V. F., Duarte, C. M., Losno, R., Sciare, J., Voss, K. J., Kinne, S., Nalli, N. R., Joseph, E., Krishna Moorthy, K., Covert, D. S., Gulev, S. K., Milinevsky, G., Larouche, P., Belanger, S., Horne, E., Chin, M., Remer, L. A., Kahn, R. A., Reid, J. S., Schulz, M., Heald, C. L., Zhang, J., Lapina, K., Kleidman, R. G., Griesfeller, J., Gaitley, B. J., Tan, Q., and Diehl, T. L.: Maritime aerosol network as a component of AERONET – first results and comparison with global aerosol models and satellite retrievals, Atmos. Meas. Tech., 4, 583–597, https://doi.org/10.5194/amt-4-583-2011, 2011.

Stein, A. F., Draxler, R. R., Rolph, G. D., Stunder, B. J. B., Cohen, M. D., and Ngan, F.: NOAA's HYSPLIT Atmospheric Transport and Dispersion Modeling System, Bull. Am. Meteorol. Soc., 96, 2059 – 2077, https://doi.org/10.1175/BAMS-D-14-00110.1, 2015.

Stocker, T., Qin, D., Plattner, G.-K., Tignor, M., Allen, S., Boschung, J., Nauels, A., Xia, Y., Bex, V., and Midgley, P.: Climate Change 2013: The Physical Science Basis. Contribution of Working Group I to the Fifth Assessment Report of the Intergovernmental Panel on Climate Change. , Cambridge University Press, ISBN 9780521705967, 2013.

Struthers, H., Ekman, A. M. L., Glantz, P., Iversen, T., Kirkevåg, A., Mårtensson, E. M., Seland, Ø., and Nilsson, E. D.: The effect of sea ice loss on sea salt aerosol concentrations and the radiative balance in the Arctic, Atmos. Chem. Phys., 11, 3459–3477, https://doi.org/10.5194/acp-11-3459-2011, 2011.

Toledano, C., González, R., Fuertes, D., Cuevas, E., Eck, T. F., Kazadzis, S., Kouremeti, N., Gröbner, J., Goloub, P., Blarel, L., Román, R., Barreto, A., Berjón, A., Holben, B. N., and Cachorro, V. E.: Assessment of Sun photometer Langley calibration at the high-elevation sites Mauna Loa and Izaña, Atmos. Chem. Phys., 18, 14 555–14 567, https://doi.org/10.5194/acp-18-14555-2018, 2018.

Torres, B., Dubovik, O., Toledano, C., Berjon, A., Cachorro, V. E., Lapyonok, T., Litvinov, P., and Goloub, P.: Sensitivity of aerosol retrieval to geometrical configuration of ground-based sun/sky radiometer observations, Atmos. Chem. Phys., 14, 847–875, https://doi.org/10.5194/acp-14-847-2014, 2014.

Tulet, P., Van Baelen, J., Bosser, P., Brioude, J., Colomb, A., Goloub, P., Pazmino, A., Portafaix, T., Ramonet, M., Sellegri, K., Thyssen, M., Gest, L., Marquestaut, N., Mékiès, D., Metzger, J.-M., Athier, G., Blarel, L., Delmotte, M., Desprairies, G., Dournaux, M., Dubois, G., Duflot, V., Lamy, K., Gardes, L., Guillemot, J.-F., Gros, V., Kolasinski, J., Lopez, M., Magand, O., Noury, E., Nunes-Pinharanda, M., Payen, G., Pianezze, J., Picard, D., Picard, O., Prunier, S., Rigaud-Louise, F., Sicard, M., and Torres, B.: MAP-IO: an atmospheric and marine observatory program on board *Marion Dufresne* over the Southern Ocean, Earth Syst. Sci. Data, 16, 3821–3849, https://doi.org/10.5194/essd-16-3821-2024, 2024.

Twomey, S.: The Influence of Pollution on the Shortwave Albedo of Clouds, J. Atmos. Sci., 34, 1149 – 1152, https://doi.org/10.1175/1520-0469(1977)034<1149:TIOPOT>2.0.CO;2, 1977.

Unga, F., Popovici, I., Dubois, G., Blarel, L., Pikridas, M., Vouterakos, P., Sciare, J., Goloub, P., Torres, B., Victori, S., Maupin, F., Canini, M., Mortier, A., and Lelieveld, J.: Mobile ship-borne sun/sky/lunar photometer and ceilometer observations during the AQABA campaign., in: Geophys. Res. Abstr., vol. 21, p. 15180, https://meetingorganizer.copernicus.org/EGU2019/EGU2019-15180.pdf, 2019.

Van den Heever, S. C., Carrió, G. G., Cotton, W. R., DeMott, P. J., and Prenni, A. J.: Impacts of Nucleating Aerosol on Florida Storms. Part I: Mesoscale Simulations, J. Atmos. Sci., 63, 1752 – 1775, https://doi.org/10.1175/JAS3713.1, 2006.

Verreyken, B., Amelynck, C., Brioude, J., Müller, J.-F., Schoon, N., Kumps, N., Colomb, A., Metzger, J.-M., Lee, C. F., Koenig, T. K., Volkamer, R., and Stavrakou, T.: Characterisation of African biomass burning plumes and impacts on the atmospheric composition over the south-west Indian Ocean, Atmos. Chem. Phys., 20, 14 821–14 845, https://doi.org/10.5194/acp-20-14821-2020, 2020.

Vigouroux, C., Stavrakou, T., Whaley, C., Dils, B., Duflot, V., Hermans, C., Kumps, N., Metzger, J.-M., Scolas, F., Vanhaelewyn, G., Müller, J.-F., Jones, D. B. A., Li, Q., and De Mazière, M.: FTIR time-series of biomass burning products (HCN, C_2H_6, C_2H_2, CH_3OH, and HCOOH) at Reunion Island (21° S, 55° E) and comparisons with model data, Atmos. Chem. Phys., 12, 10 367–10 385, https://doi.org/10.5194/acp-12-10367-2012, 2012.

Yin, Z., Ansmann, A., Baars, H., Seifert, P., Engelmann, R., Radenz, M., Jimenez, C., Herzog, A., Ohneiser, K., Hanbuch, K., Blarel, L., Goloub, P., Dubois, G., Victori, S., and Maupin, F.: Aerosol measurements with a shipborne Sun–sky–lunar photometer and collocated multiwavelength Raman polarization lidar over the Atlantic Ocean, Atmos. Meas. Tech., 12, 5685–5698, https://doi.org/10.5194/amt-12-5685-2019, 2019.